University of Utrecht

Full vector geomagnetic field record of 28 lava flows from El Hierro, Canary Islands, Spain

Author:
J. P. van Galen, BSc

Supervisors:
M.W.L. Monster, MSc
Prof. dr. C.G. Langereis

Netherlands Organisation for Scientific Research

Paleomagnetic Laboratory Fort Hoofddijk

Department of Earth Sciences
Budapestlaan 17, 3584 CD Utrecht
The Netherlands

January 20, 2015

Abstract

Direct observations on the Earth's magnetic field have only been done during the last 170 years, finding a gradual decline over this period. Attempts to increase the temporal and spatial constraints for the paleofield are made by looking at archaeological sites. Models based on these sites give spatially limited insight in the behavior of the field in the last 7 kyr. In order to obtain global paleointensity coverage new and improved methods have been conducted on volcanic islands predominantly on the northern hemisphere. Here, paleodirections were obtained from lavas flows El Hierro, Canary Islands, Spain. In addition, three different intensity methods were used to obtain information about the full-vector field. An age model was created (middle to late Brunhes 466 - 135 ka) based on a stratigraphic and directional coherency with a dated section 4 km northwest. The directions in this study and in the published section 4 km northwest deviate east around $\sim$ 13 $^{\circ}$. These eastern directions in both studies are attributed to unrepresentative sampling to properly depict paleosecular variation. Thellier-Thellier, the recently proposed multi-speciment parallel differential pTRM method combined with the ARM-test, and the very recent Pseudo-Thellier approach are here thoroughly reviewed on success rate, workload and results. A paleointensity trend is suggested with intensities often $\sim$15 μT lower than the current intensity for El Hierro ($\sim$ 39 μT), showing only three phases of intensities equal or close to present day values.

Contents

Introduction

The origin of the Earth's magnetic field is found in the interaction between the solid inner core and the convection currents in the liquid outer core. The field protects the Earth from harmful background and solar radiation, and is of vital importance for modern technology. Little is known, however, about the variations of the Earth's magnetic field and the rate of change that can be expected. Known is that the field has been declining in strength in the 170 years (De Groot et al., 2013a) that there are measurements, but there is no consensus on the field intensities that can be expected during a stable polarity.

Data that can increase the temporal and spatial coverage can be obtained from materials that cooled in the Earth's magnetic field, thus storing its signal as a natural remanent magnetization (NRM). This occurs at archaeological sites, where re-heating of material is temporally well defined. These archaeological sites are mostly found in Europe (Gallet et al., 2002), the Middle-East (Ben-Yosef et al., 2012; Gallet & Le Goff, 2006; Shaar et al., 2011) and North America. This made it possible to create models of the field in the last 7 kyr (Korte & Constable, 2005; Korte et al., 2005; Pavón-Carrasco et al., 2010), covering these locations. Sediments have been used to obtain relative intensities (e.g. Tauxe et al., 1995; Yang et al., 2012). Sediments are limited in temporal perspective since sedimentation rates are often very low. Sediments generally contain very few magnetic minerals and exhibit poor signals.

In an effort to increase the global spatial and temporal coverage of the paleointensities, work is done on continental volcanic regions and oceanic sedimentary and basaltic cores (e.g. Langereis et al., 1997; Ravilly et al., 2001). Often visited locations are volcanic and hotspot islands. Studies have been done in Hawaii (De Groot et al., 2013a; Laj & Kissel, 1999; Laj et al., 2011), the Azores (Di Chiara et al., 2014), Iceland (Muxworthy & Taylor, 2011), Mediterranean islands (De Groot et al., 2013b; Spassov et al., 2010) and remote islands like Amsterdam Island (Singer, 2014) and New Zealand (Cassidy & Hill, 2009). Work is done on the Canary Islands (Valet & Soler, 1999), La Palma (De Groot et al., 2012; Quidelleur & Valet, 1996), Tenerife (Kissel et al., 2011) and Grand Canaria (Leonhardt & Soffel, 2002) with a focus on recent reversals or excursions. The region lacks studies on the stable dipolar field. On the island of El Hierro there is one high resolution directional study done (Széréméta et al., 1999), and no intensity work.

In order to get better constraints on the intensities and rates of change that might be expected, several methods to yield reliable paleointensities have been proposed. The

Thellier-Thellier method (Thellier & Thellier, 1959) is the first attempt to derive paleointensities from (volcanic) rocks. Additions and variations to this technique (Coe et al., 1978; Leonhardt et al., 2004; Riisager & Riisager, 2001; Yu & Tauxe, 2005) have improved it since. New methods have been introduced recently, the microwave method (Hill & Shaw, 1999), the multi-specimen protocol (Dekkers & Böhnel, 2006; Fabian & Leonhardt, 2010), and Pseudo-Thellier (De Groot et al., 2013a). This in an attempt to increase the number of methods available, obtain more reliable data, increase the success rate and reduce the workload. However, very little work is done comparing these methods (De Groot et al., 2013a; Muxworthy & Taylor, 2011).

In this work three methods have been applied, the Thellier-Thellier method, the multi-specimen protocol (Dekkers & Böhnel, 2006; Fabian & Leonhardt, 2010) and pseudo-Thellier (De Groot et al., 2013a). These methods are compared in terms of workload and reliability and the results. It will increase the work done on the more recently proposed methods and enables comparison. This study will furthermore attempt to find, confirm and explain directional anomalies found by Széréméta et al. (1999). It will explore the extremes expected in a stable polarity, and show the results and problems associated with a multi-protocol approach to a paleointensity study.

Chapter 1

Geological Setting & Sampling

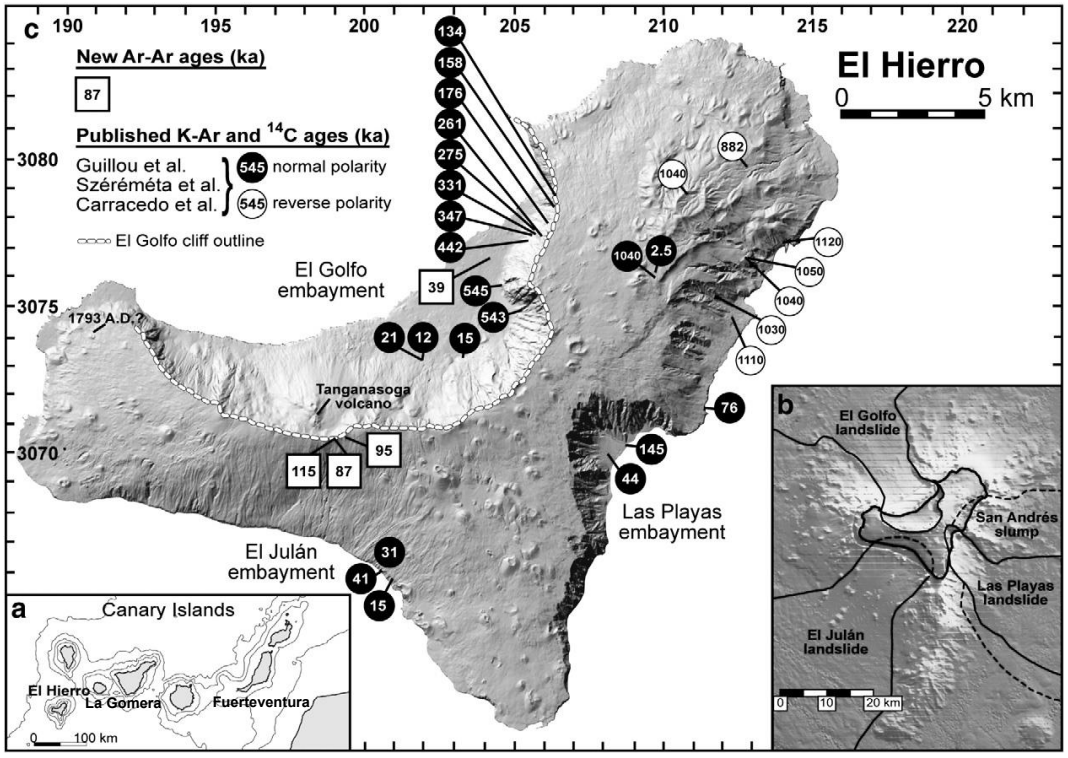

Figure 1.1: a) Map of the archipelago. b) Shaded submarine topography map of El Hierro showing all deposits and correlated landslides. c) El Hierro (UMT, WGS84) containing all ages from (Carracedo et al., 2001; Guillou et al., 1996; Longpré et al., 2011; Széréméta et al., 1999) and the sampling locations from this study. All figures after Longpré et al. (2011).

The Canary Islands (figure 1.1a) are an east-west oriented island group about 200 kilometers west of the north African coast. It consist of seven main islands that rise approximately 4000 m from the sea floor. The archipelago formed during the early Miocene (Gee et al., 2001) as a result of the presence of a mantle plume hotspot

(Guillou et al., 1996; Holik et al., 1991). The westernmost islands are the youngest, with Fuerteventura the oldest (<20 Ka) and El Hierro most recent (>2 Ma) (Gee et al., 2001). Only La Gomera's position is anomalous with an age of 12 Ma, it is the only island in the group that was not volcanically active the last 5 kyr (Gee et al., 2001).

The oldest dated rocks on El Hierro (figure 1.1b) are 1.12 Ma (Guillou et al., 1996) and were found in the northeast of the island, near the village of Tiñor. Most of the island is covered by more recent lavas coming from the western El Golfo volcano (Carracedo et al., 2001) covering the older lavas. A hiatus in dated lavas (882-545 ka) between the northeastern Tiñor and the western El Golfo regions suggest a break in volcanic activity. This is attributed to the development of a dual-line volcanic system between La Palma and El Hierro in this same period (Carracedo et al., 2001). Carracedo et al. (2001) & Széréméta et al. (1999) have observed two phases of volcanism within the El Golfo volcano, starting with an initial El Golfo stage (dated >261 ka) and a later stage of rift volcanism (dated <176 ka). These authors interpret a thick red sedimentary layer in between these two phases as evidence for a period of volcanic inactivity.

The El Golfo embayment is a relict of one of many massive landslides that dominate the submarine and terrestrial characteristics of the island of El Hierro (figure 1.1b) (Carracedo et al., 2001; Gee et al., 2001; Longpré et al., 2011). Enormous blocks up to 1.2 km across and 200 m high, found in a 1500 km^2 area have been identified as part of the collapsed El Golfo volcano. Sediment on top of these deposits have been dated, suggesting the scarp formed between 10 and 17 ka (Masson, 1996). Sub-horizontally deposited lavas at the highest point of the island, believed to be the youngest pre-collapse flows found, with an age of 84 ka. Lavas dipping at an angle of approximately 30° inside the embayment, the oldest post-collapse lavas, are not found older than 38 ka (Longpré et al., 2011). There is no bathymetric evidence for more than one El Golfo collapse event (Longpré et al., 2011), thus the discrepancy between the two approaches remains a topic of discussion.

The steep slopes of the El Golfo cliffs consist of many individual lava deposits, tephra layers and some paloesols. For this study the path leading from the Calle los Corchos, north of La Frontera, up to Mirador De Jiñama was used as a sampling location (figure 1.1b). A total of 28 separate lava flows (figure 1.2) were sampled, using a petrol-powered drill. A total of 10 to 20 cores were drilled per site, some oriented to obtain directions, other (hand)-samples without orientation for paleointensity and dating purposes. When possible, both solar and magnetic compasses were used to orient the cores. The difference between the solar and magnetic compass was generally below 10 °, with the exception of site 13 which is believed to have been struck by lightning.

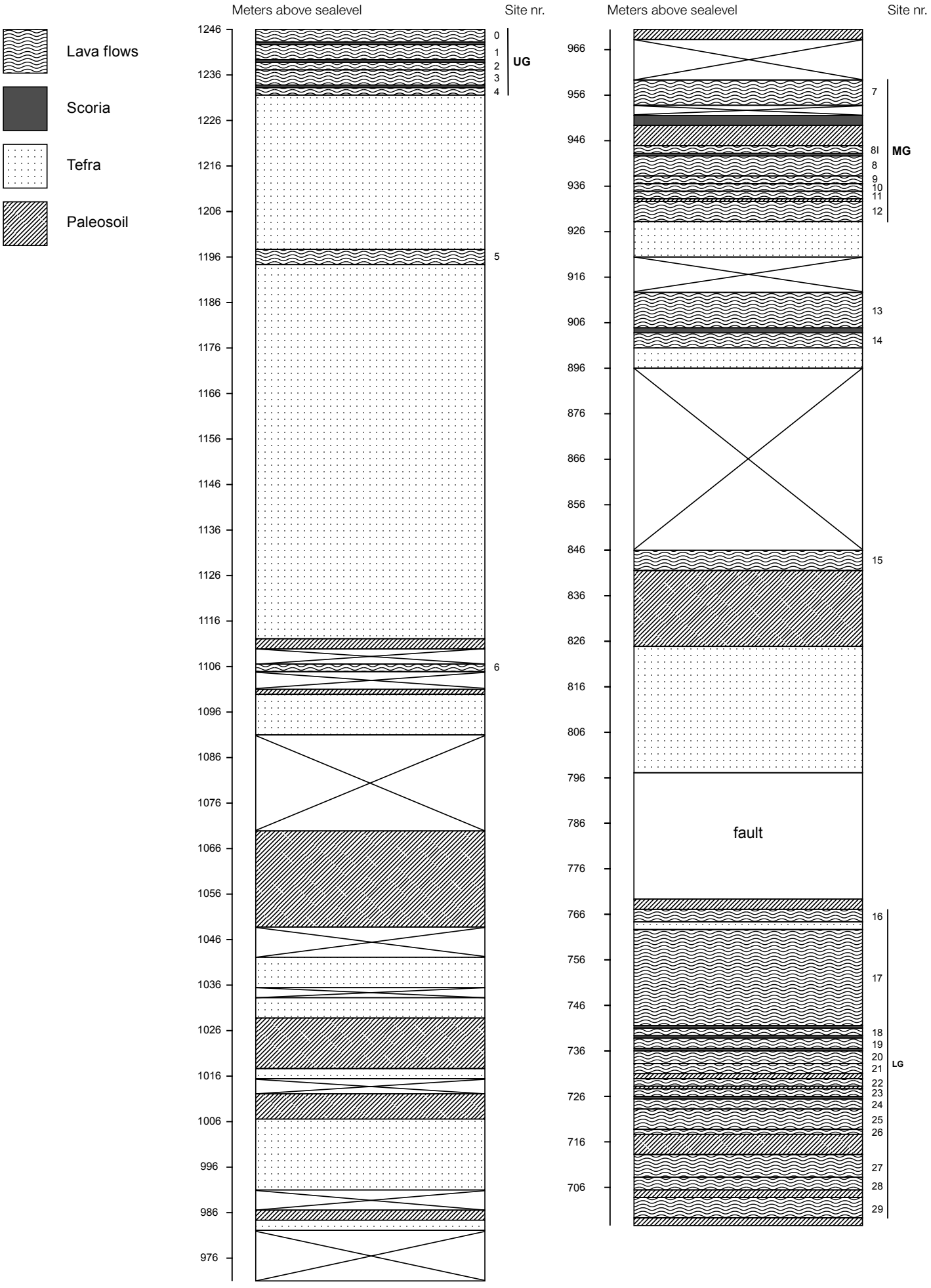
Lava flows
Scoria
Tefra
Paleosoil
Meters above sealevel
Site nr.
1246
1236
1226
1216
1206
1196
1186
1176
1166
1156
1146
1136
1126
1116
1106
1096
1086
1076
1066
1056
1046
1036
1026
1016
1006
996
986
976
0
1
2
3
4
UG
5
6
Meters above sealevel
Site nr.
966
956
946
936
926
916
906
896
876
866
856
846
836
826
816
806
796
786
776
766
756
746
736
726
716
706
7
8l
8
9
10
11
12
MG
13
14
15
fault
16
17
18
19
20
21
22
23
24
25
26
27
28
29
LG

Figure 1.2: All 28 sampled lava flows, in stratigraphic groups, upper group (UG), middle group (MG), and lower group (LG). Site 0 was to brittle to drill, sites 5 and 15 were unsafe to sample. Site 6, 13 and 14 are not allocated to one of the groups. The fault just above LG is interpreted as dip-dip fault parallel to the rock face which occurred after the El Golfo collapse. An estimated 30 m of stratigraphy was covered here. No duplication in the underlying sequence was observed.

Chapter 2

Methods

2.1 Rock-Magnetic & Paleomagnetic Methods

2.1.1 Alternating Field Demagnetization

Using alternating fields (AF) to demagnetize samples is a common method to determine the direction of magnetic north at the time of rock formation. It is also used to check whether a sample has a magnetic overprint, which is important for the conduction of some of the paleointensity experiments described in section 2.2.3 and 2.2.2.

The natural remanent magnetism (NRM) was AF demagnetized using a robotized 2G DC-SQUID magnetometer with increasing field steps of 0, 2.5, 5, 7.5, 10, 15, 20, 25, 30, 40, 50, 60, 70, 80, 90, and 100 mT. Three additional steps of 150, 225 and 300 mT were manually conducted, due to the technical imitations of the robotized magnetometer. After the 300 mT step the magnetization was generally reduced to only a few percent of its NRM.

2.1.2 Thermal Demagnetization

Thermal (TH) demagnetization is based on the correlation between relaxation time and temperature. If the relaxation time of a given magnetic particle is shorter than the laboratory heating process the particle will be magnetically unblocked. The particles that have the shortest relaxation times are unblock first, which are the particles that have the biggest chance of having a secondary magnetization. In a zero field environment the particle will order itself according to its principle axis, hence the particles' magnetization is randomized. The temperature at which this process starts, depends on grain size and domain state (see section 2.2.1). For this

reason we see a gradual demagnetization when samples are stepwise heated to higher temperatures (Tauxe, 2010).

The NRM of three samples per site were measured before they were heated to temperatures of 100, 150, 200, 250, 300, 250, 400, 450, 500, 525, 550, and 580 °C. For samples that had lost more then ±20% of their NRM at 100 °C the 150 °C step was replaced by a 130°C and a 160°C step. Samples with an NRM higher than $\pm 8 Am^{-1}$ were measured using a AGICO JR-6 spinner magnetometer (low speed, three-position semi-automatic holder). Weaker samples were measured on a manual 2G DC SQUID magnetometer. All demagnetization steps were conducted using a ASC TD-48 SC thermal demagnetizer.

2.1.3 Magnetic Susceptibility

Magnetic susceptibility is a dimensionless quantity that shows how responsive a material is to an induced magnetic field. In the lavas that are studied here, this is considered a material property. Magnetic susceptibility can be formulated as follows:

$M = \chi H$

χ = magnetic suseptibility
M = samples' magnetization (A/m)
H = applied field (A/m)

The susceptibility was measured as a function of temperature on a AGICO KLY-3 Kappabridge pickup system. About half a gram of powdered material was exposed to ten temperature paths. The material was heated to 150 and cooled to 100 °C. After this the material was repeatedly heated a 100 and cooled 50 °C. When it had reached 600 °C is was cooled to room temperature. The results of these experiments can be found in figure 3.3 and in section A.

2.1.4 Magnetic Hysteresis

The magnetic hysteresis is the memory of a rocks magnetization against an induced magnetic field. When samples are exposed to a laboratory field (H) the material acquires a magnetization (M) whilst it stays in this environment. When the field is reduced, the magnetization of the material decreases along with it. However, the magnetization and the field do not behave linearly; when the field is zero, the magnetization of the samples is not (figure 2.1). When the field reaches zero the direction of the field is reversed after which it reaches maximum value before going back to zero again. A symmetric looped figure is plotted; a hysteresis loop. The distance between the values of M for H = 0 is twice the coercivity of the material. The coercivity is expressed in A/m and is a quantity for resistance to AF demagnetization (section 2.1.1).

Cylindrical samples with a diameter and length of 8 mm were drilled from the cores. These samples were measured using a VSM magnetometer with fields of +1.5 T to

-1.5 T. After this a back-field curve measurement was conducted to find the saturation magnetization, with the VSM going up to 0.53 T. With the results from these measurements the ratios of M_r/M_s, and H_c/H_r, a Day plot was created (Day et al., 1977, figure 3.4) to get insight in the magnetic domain state of the lavas.

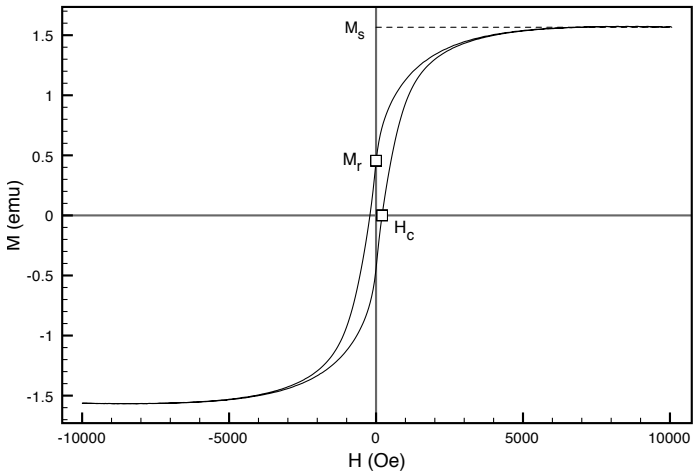

Figure 2.1: A hysteresis loop with the applied field H on the x-axis, and the magnetization M of the sample on the y-axis. The distance between the two x-axis crossing points is twice the coercivity. Image courtesy of M.W.L. Monster

2.2 Paleointensity Methods

2.2.1 Thellier-Thellier

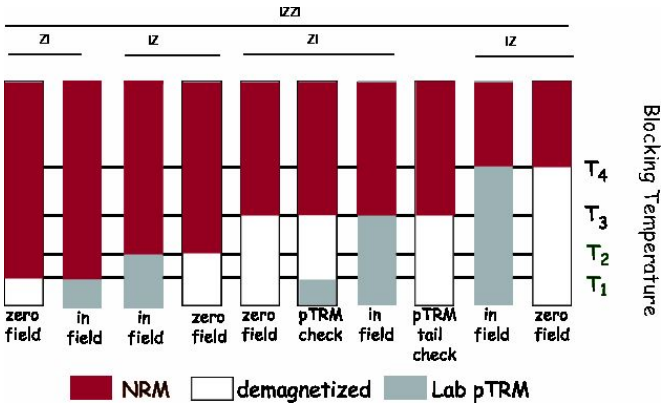

Figure 2.2: The IZZI protocol (Yu et al., 2004) showing all steps and checks performed in this study. Figure from Tauxe (2010)

The classic Thellier-Thellier type experiment, developed by Thellier & Thellier (1959) forms the basis of the current standard of paleointensity determination. In the original protocol samples were heated twice, with laboratory fields in opposite directions. Improvements on is method by Aitken et al. (1988); Coe et al. (1978), led to the so called "zero-field/in field, "ZI" en "IZ" protocols. This requires samples to cool in a zero field environment making it easier to compare the NRM remaining with the pTRM gained. Aitken et al. (1988)'s protocol compensated for the so called "zero field memory effect".

These methods work on Thellier's principal assumption that NRM lost can be fully and independently replaced by a pTRM. This is only true in the ideal situation that all the NRM and pTRM are carried by single-domain (SD) particles. In practice magnetite and titanomagnetite, common magnetic carriers, show pseudo-single-domain (PSD) and multi-domain (MD) behavior when heated, making them untrustworthy as a paleofield recorder (for a thorough review on SD, PSD and MD behavior see e.g. Dunlop & Xu (1994); Xu & Dunlop (1994)). Riisager & Riisager (2001) proposed a "pTRM tail check" to identify samples that show MD behavior and remove the ones that may give unreliable paleointensities. This check consists of a third heating phase in zero field added to the method by Coe et al. (1978).

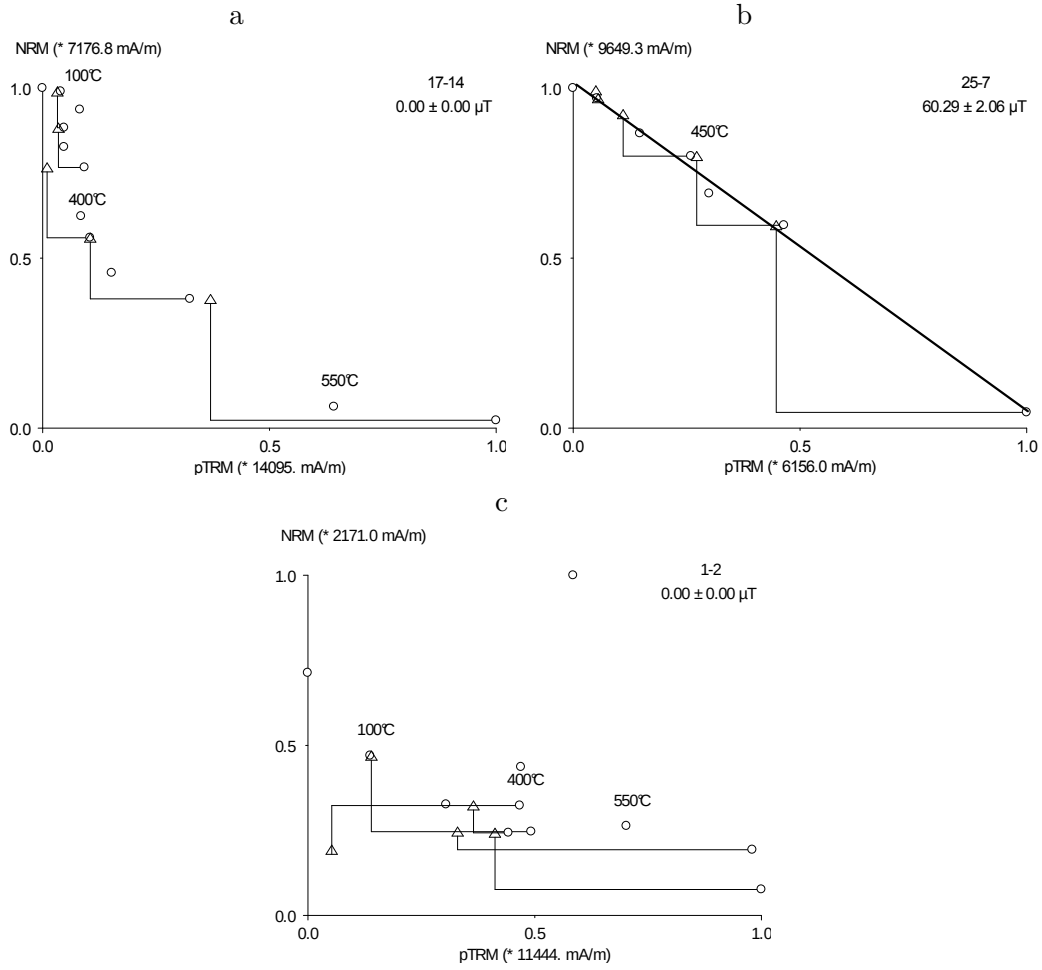

Figure 2.3: Arai plots (Nagata et al., 1963) showing typical Thellier-Thellier results, with the paleointensity in the right top corner. Circles show the NRM as a function of pTRM at a given temperature. Triangles depict the pTRM checks, connected to the position from which the check was conducted. a) A plot from site 17 showing "sagging" caused by MD behavior. b) Figure from site 25 showing very linear behavior, and good pTRM checks, passing the B criteria. c) Site 1 shows very complex behavior making it very difficult to interpret. All plots were made using ThellierTool 4.0 (Leonhardt et al., 2004).

Both the Coe, and the Aitken methods yields very different outcomes when conducted separately (Yu et al., 2004). Yu et al. (2004) propose the "IZZI" (figure 2.2) protocol, a combination of Coe's and Aitken's method, in order to minimize the angular dependency of the used laboratory field. This method, the "IZZI" protocol with pTRM tail checks, thoroughly tested by Yu & Tauxe (2005), is used in this study.

The thermal demagnetization treatment was conducted using a ASC TD-48 SC thermal demagnetizer. Strong samples were measured on a AGICO JR-6 spinner mag-

netometer. Weaker samples were measured on a 2G DC SQUID magnetometer. Analysis was done with ThellierTool (Leonhardt et al., 2004, see figure 2.3) using the included TiellierTool A/B selection criteria.

2.2.2 ARM Test & Multispecimen Protocol

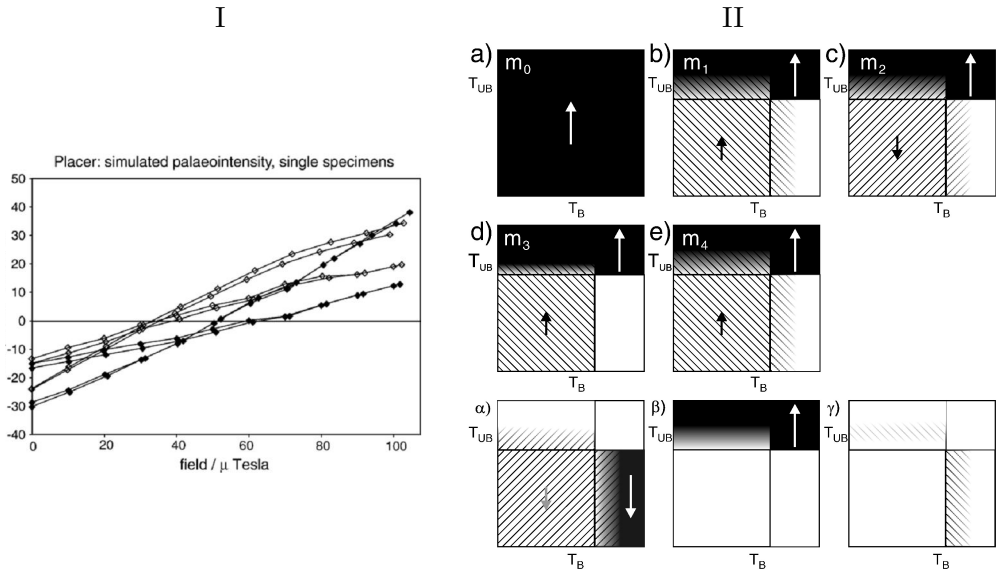

Figure 2.4: I) Simulated plot from Dekkers & Böhnel (2006) showing H_{lab} on the x-axis and the Q_{DB} on the y axis. When the Q_{DB} is 0 we find the H. In this simulation multiple specimens were subjected to eleven field steps. In this study there were five. II) A phenomenological visualization of the MSP-DSC protocol from Fabian & Leonhardt (2010) showing all five steps. α renders the traditional DB protocol ($(a-b)/2$) which β shows the slope correction ($(b+c)/2$). γ is a measure for thermo-chemical and domain state alteration ($(a-e)/2$), and is used to determine of the MSP-DSC can be used or if the MSP-DB might yield more reliable results.

The classical Thellier-Thellier method for paleointensity determination as described in section 2.2.1 has been used for decades, but it has some inherent limitations. The theory is correct if all carrier are in SD, but in reality PSD and MD carriers are found (Dunlop & Xu, 1994; Xu & Dunlop, 1994). This leads to "sagging" and otherwise unreliable Arai plots (figure 2.3). Another requirement of this method is that samples have to be heated in several steps to temperatures above their Curie-temperature (i.e. Coe et al. (1978); Thellier & Thellier (1959)). This may induce chemical altered causing the samples to fail the checks developed to detect the possible error sources, leading to a very low success rate.

In order to obtain reliable intensity data for more sites than in the classical Thellier-Thellier method, a new protocol was proposed by Dekkers & Böhnel (2006); the multi-

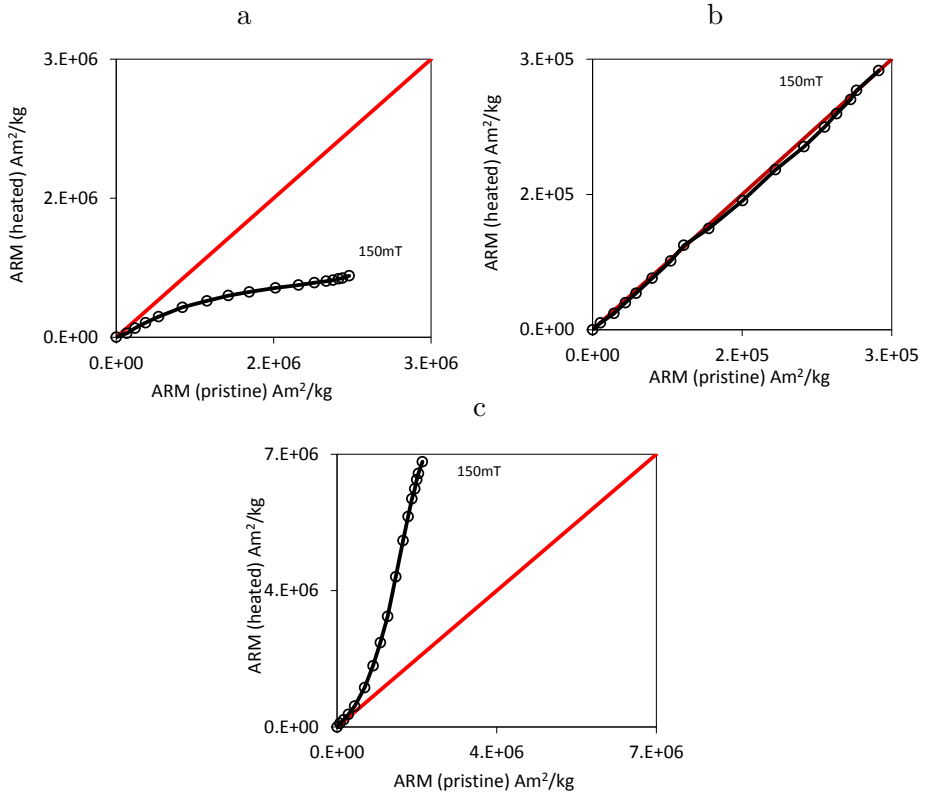

Figure 2.5: Acquisition experiments, showing three different behaviors. a) Site 26 acquires less ARM after heating, b) Site 11 doesn't show difference in ARM acquisition. c) Site 27 picks up more ARM after heating.

specimen parallel differential pTRM method (MSP-DB). The principle behind this approach is based on the linearity and domain state independence of the pTRM with an induced field. The laboratory pTRM was acquired in the same direction as the original NRM, which is considered to be a full TRM. This makes scalar subtraction easier, and it reduces errors due to tail effects. The further elegance of the protocol is found in the simple relation between the laboratory induced field (H_{lab}) and the ancient paleofield (H_{anc}) in which the NRM has been acquired. When $H_{lab} = H_{anc}$ we do not expect a difference in the pTRM + $NRM_{remaining}$ component (Q_{DB})(See figures 2.4I & IIα), while we expect $H_{lab} > H_{anc}$ when Q_{DB} is negative. Another advantage is that the temperature of the single heating step at which the experiment is conducted can be chosen freely and below its alteration temperature, reducing the risk of alteration (Dekkers & Böhnel, 2006).

Fabian & Leonhardt (2010) found in both modelling and laboratory work that the protocol proposed by Dekkers & Böhnel (2006) still yielded overestimates of the paleofield for particles in the PSD and MD state, hence the MSP-DB protocol was

not domain state independent. In order to correct for these problems several steps were added to the MSP-DB protocol (Fabian & Leonhardt (2010), figure 2.4IIa-e):

m0 The NRM is measured, the declination and inclinations are used to align the samples with the laboratory field. (Figure 2.4 IIa (MSP-DB))

m1 The samples are heated and cooled in parallel field. (Figure 2.4 IIb (MSP-DB))

m2 The samples are heated and cooled in an anti-parallel field. (Figure 2.4 IIc (MSP-DSC))

m3 The sampels are heated in zero field and cooled in a parallel field. (Figure 2.4 IId (MSP-DCS))

m4 Step 2 is repeated. (Figure 2.4 IIe (MSP-DSC))

The calculation of the Q_{DSC} factor from the results obtained in these measuring steps relate as follows:

$$Q_{DSC} = \frac{(1+\alpha)m_1 - m_0 - \alpha m_3}{2m_0 - m_1 - m_2}$$

Fabian & Leonhardt (2010) found problems caused by the multiple heating cycles, leading to thermo-chemical and domain-state alteration causing the magnetic properties to become irreversible, and thus incomparable. In order to overcome this drawback Fabian & Leonhardt (2010) asked for a test that could improve the reliability of these experiments by choosing a temperature at which no magnetic alteration occurs. De Groot et al. (2012) proposed this test and added it the to work flow of Fabian & Leonhardt (2010) so that sites that yield reliable paleointensities can be selected base on their alteration properties. This single-core anhysteretic remanent magnetization (ARM) acquisition experiment by De Groot et al. (2012) was used in this study.

Eight samples were prepared. When material was available from one single core, more often from two. The cores (2.5 cm diameter) were cut into thick half circles. Four of these samples were partially thermally demagnetized in a singles heating step. The four others remained in the pristine NRM state. The unheated samples always came from the same cores, the same goes for the heated samples. The temperature to which the samples were heated was obtained from the magnetic susceptibility experiments in section 2.1.3. The temperature is chosen below a point at which non reversible behavior occurs but high enough that the sample lose at least some 10% of the NRM. Sites with a magnetic overprint were based on the thermal demagnetization rejected (section 2.1.2) decay plots in figure 3.3. Two of the heated and two of the pristine samples were stepwise demagnetized to 150 mT (see section 2.1.1) where only one axis is considered, being the one parallel to the length of the core (x-axis). The four

remaining specimens were subjected to the same singles-axis AF demagnetization, but in this case whilst subjected to a 40μT DC bias field, leading a ARM acquisition.

All four sample couples (AF demag/pristine, AF demag/heated, ARM acq./pristine, ARM acq./heated) were averaged. Only the x-axial intensities were considered and normalized by mass. The ARM acquisition series were subtracted from the AF demagnetized series. Several further steps were taken to create a corrected data series. An NRM scatter correction is applied, and the 0-μT-series' remaining magnetization were set to zero. For more extensive dilatation regarding the single-core ARM acquisition see De Groot et al. (2012).

Figure 2.5 shows three ARM acquisition curves, with pristine samples on the x-axis and heated on the y-axis. In plot b, the ARM acquisition of the heated and the pristine samples is equal and plots on the ideal x = y line, indicating no alteration and the test is passed. Figure 2.5a shows an examples of a site that acquires less ARM after heating (plots below x = y), whilst the figure 2.5c acquires more ARM (plots above x = y). If an ARM is acquired easier after heating (figure 2.5c) the paleofield will be underestimated in an MSP experiment. Otherwise, if a sample acquires an ARM with difficulty after heating, the result will be an overestimate. Note here that an MSP experiment should only be conducted at the temperature at which it passed the ARM-test, since it might fail even at a lower temperature (M.W.L. Monster, personal communication).

Standard field steps are 12, 24, 36, 48 and 60 μT, with the exception of site 11 (12, 36, 60 and 84 μT). All field steps were conducted in a ASC TD-48 SC thermal demagnetizer; a (portable) power source was used to apply the field. After each step all samples were measured on a AGICO JR-6 spinner magnetometer (low speed, three-position semi-automatic holder).

2.2.3 Pseudo-Thellier

The Pseudo-Thellier technique is known to yield relative paleointensity data in sediments (Tauxe et al., 1995) and is inspired by the traditional paleointensity method by Thellier & Thellier (Thellier & Thellier, 1959), later enhanced by Coe (Coe et al., 1978). When using this technique on sediments, a limitation in data that can be obtained is apparent. Knowing the sedimentation rate of a given type of sediments (Tauxe et al., 1995) the variation in the stored magnetic signal (both directions and intensities) is smoothed in the sample and correlated time interval. When working with lavas this problem does not occur, since the sampled cores store the magnetic signal as a "snapshot". This is where the analogy between the Pseudo-Thellier and the thermal Thellier method can be found. The NRM demagnetization can be compared to the acquired ARM, assuming that the magnetic grains of the NRM (a full TRM) are the same as those for the ARM. This was studied by Yu et al. (2003) and a strong grain size dependency on the TRM/ARM ratio was found. Here we conduct the Pseudo-Thellier method (De Groot et al., 2013a). It compares the NRM

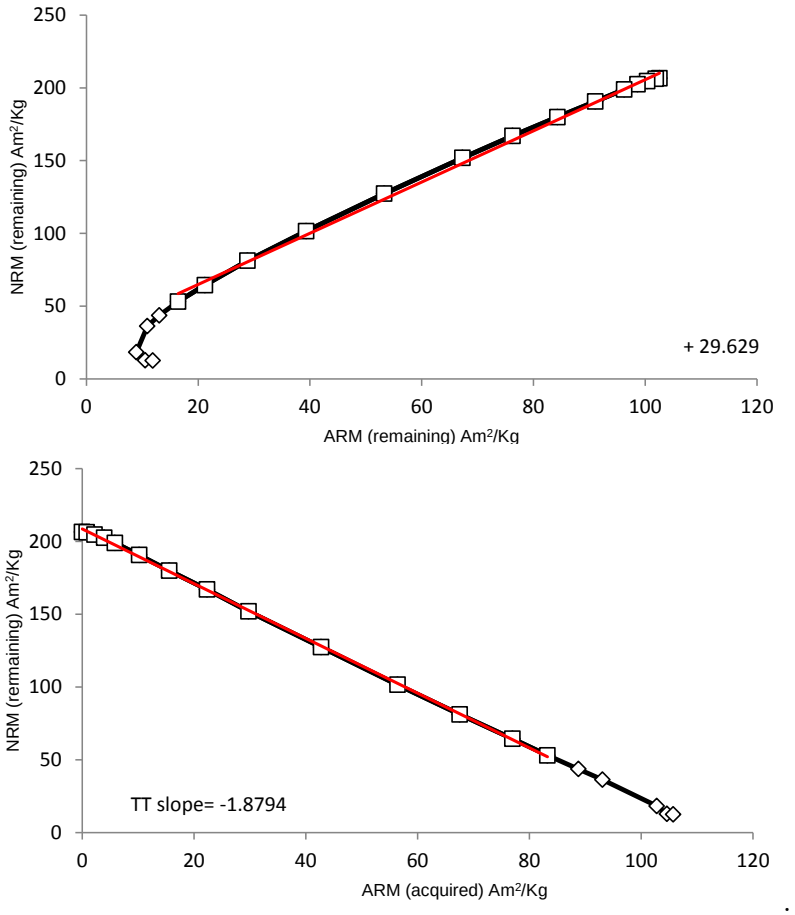

Figure 2.6: Site 22: Weight normalized ARM & NRM (top) and Arai plot (bottom) with linear fit over alternating field steps of 40mT to 300mT. Pseudo-Thellier slope and y-axis interception are plotted in the figures.

demagnetization with an ARM acquisition and demagnetization. These three steps are listed below.

- The samples were AF demagnetized (section 2.1.1)
- The acquisition of the ARM was conducted with the same field steps as in the NRM demagnetization, but the samples were exposed to a DC bias field of 40μT. The 150 mT step was conducted on the automated magnetometer. The 225 & 300 mT steps were conducted manually, in an equal 40μT DC bias field.
- The demagnetization of the ARM was conducted in the same way as the NRM demagnetization.

To select samples that yield reliable results for this method a set of empirical criteria was used (De Groot et al., 2013a). The weight normalized magnetic moment of

the ARM and the NRM are compared. A linear interval of preferably intermediate field steps is chosen to determine a slope for a linear fit and calculate the Pseudo-Thellier slope (figure 2.6). The steps are chosen so that possible overprints seen in AF demagnetization are excluded, see section 2.1.1. The same field steps are used to calculate the Pseudo-Thellier slope from an Arai plot. four tests are conducted to accept or reject the sites.

- The relation between NRM and ARM demagnetization is linear (see figure 2.6 top).
- Half the maximum ARM is acquired in a field, the $B_{1/2ARM}$. This field is found by interpolating between to measured field steps. The sample is accepted when $B_{1/2ARM}$ is between 23 and 63 mT.
- The standard deviation over the average Pseudo-Thellier slope of the samples of one site can not be more than 15%.
- All sites have 3-5 individually accepted cores.

The relation between the Pseudo-Thellier slope averages and the absolute paleointensity can be found according to empirical relation found on Hawaii by De Groot et al. (2013a):

$$B_{abs}(\mu T) = 7.371 \times \mid \text{Pseudo-Thellier slope} \mid + 14.661$$

Chapter 3

Results

3.1 Rock-magnetic & Paleomagnetic Analyses

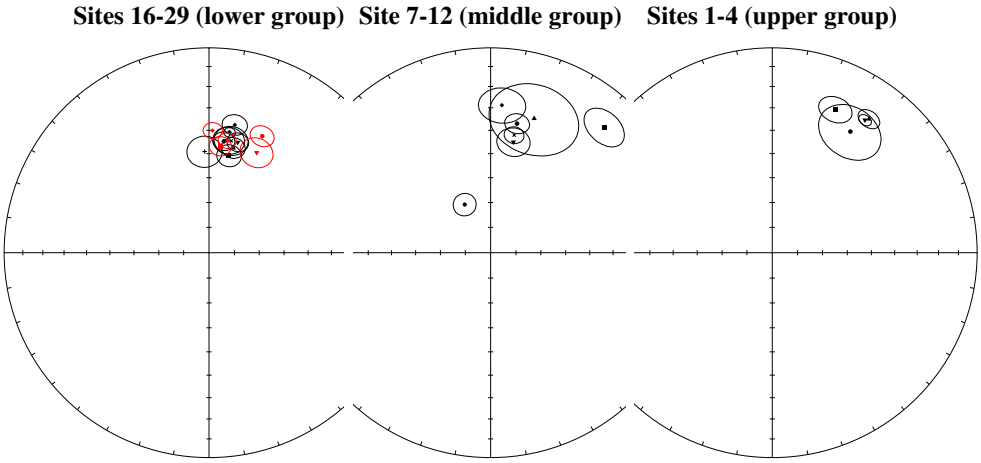

Figure 3.1: All sites have been subjected to a 45° cutoff test, giving averages and $\alpha 95$. All cores and the 45° test are plotted in Appendix B. The westward outlier in MG is site 8I, the one eats is site 9. Not plotted here are sites 6, 13 and 14 (see text).

The three groups show very similar directions, with the exception of sites 8I and 13 which are believed to have been struck by lightning (figure 3.1). In figure 3.3 very rapid AF demagnetization of the NRM can be observed for site 8I, characteristic behavior for remagnetization by lightning. Site 13 exhibits very heterogeneous behavior, as can be seen in appendix A. It has strongly varying NRMs, whose intensity can be up to 670 A/m. This makes the use of a field solar compass necessary when orientating samples, since a regular compass may be deviated significantly by the outcrop itself. Site 6, 13 and 14 are "stratigraphic islands", these sites are not shown in the three defined groups. Further notes can be made on site 1 in figure 3.3. It shows a clear overprint in the AF Zijderveld plots, which is characteristic for the sites in the UG. Another typical trait for the UG is the increase in magnetization in the AF decay plots, which can also be observed for site 11 (figure 3.3). This might be

related to the demagnetization of the overprint. The paleodirections and statistical data from all sites can be found in table 3.1, all plots can be found in appendix B.

There are two features noticeable when considering the directions for all sites is that the positions of magnetic north are east of absolute north. Only site 17 and 6 have paleodirections just west (figure 3.2). An approximate 20° steepening of the inclination seems apparent. The same general eastward trend in paleo-directions (to a lesser extent a steepening of the inclination) has been observed by Szériméta et al. (1999).

Common true mean direction (CTMD) filtering was conducted by Szériméta et al. (1999), and their work is duplicated here using the method of McFadden & McElhinny (1990), leading to the same results as seen in table 3.1. The same tests are conducted for the sites in this study (table 3.1) and it is shown that the UG only accounts for two data points after filtering. The LG shows very little scatter in figure 3.1, but the CTMD testing step does not decrease the amount of data points dramatically. Table 3.1 shows in five occasions two ore more sites are statistically indistinguishable. The 28 sampled lava flows and correlated retrieved directions are interpreted as 21 independent data points, including sites 8I and 13.

Figure 3.4 shows results of the hysteresis and back-field curve experiments, the magnetic domain state in the Day plot (Day et al., 1977). No sites fit in the SD range, but the far majority of the sites exhibit the transitional PSD behavior. Especially sites from LG show homogeneous behavior, and can be found in the center of the PSD range. Some examples in LG plot in the MD window (sites 24 and 29). UG shows quite coherent behavior, but the sites from MG vary largely in domain state. Site 8I and 11 are the nearest to true SD behavior, whilst site 7 has an extremely high H_c / H_r ratio and falls outside the plot. For these and the other sites that fall outside the PSD box, mixtures of more at least 90% MD grains are found (Dunlop, 2002).

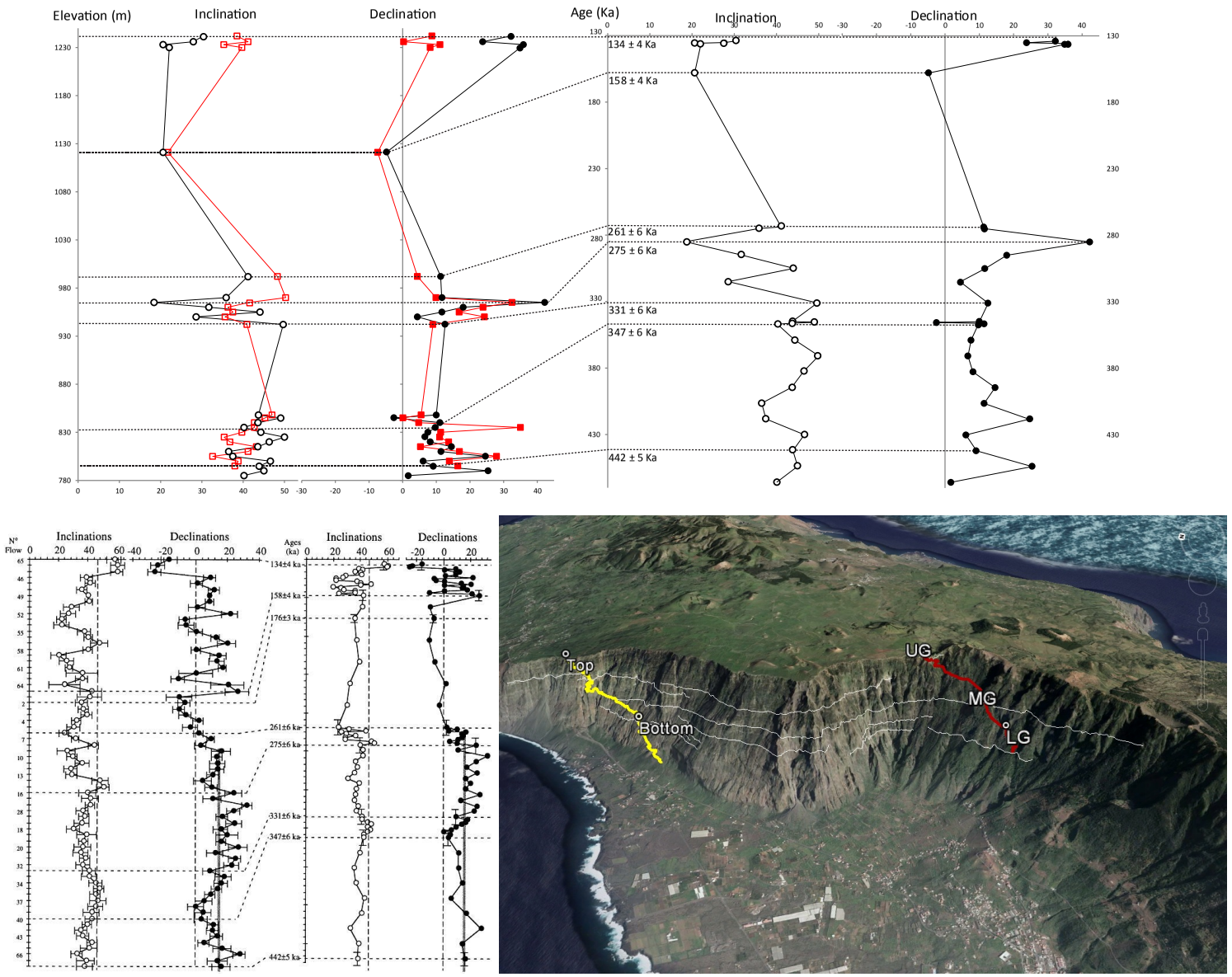

Figure 3.2: Visual representation of the created equal time per m based age model (top) with the linked sites from Széréméta et al. (1999) in red. Left plot, the directions according to Széréméta et al. (1999). Right show the geographical coherency in both this work (path in red) and that of Széréméta et al. (1999) in yellow. The top and bottom of their section are shown, as are the three defined groups in this work.

Széréméta et al. (1999)					this study							this study filtered				
sites	dec	inc	N	K	sites	dec	inc	N	K	CTMD	age (Ka)	dec	inc	N	K	age (Ka)
46	8.7	38.5	6	218.3	1	32.2	30.4	7	41.6	N	134	-	-	-	-	
47	0.3	41.2	5	340.6	2	23.8	27.8	8	25.9	N	135	27.9	29.1	15	29.8	135
48	11.1	35.3	5	478.9	3	35.9	20.6	8	320.1	N	136	-	-	-	-	
49	8.2	39.7	2	999.0	4	35.0	22.1	8	562.2	N	136	35.5	21.4	16	427.1	136
53	352.6	21.8	5	483.6	6	355.2	20.6	8	243.5	Y	158	355.2	20.6	8	243.5	158
14	4.4	48.3	7	96.6	7	11.3	41.1	8	24.2	Y	261	11.3	41.1	8	24.2	261
-	-	-	-	-	8I	331.4	68.2	5	108.8	-	275	331.4	68.2	5	108.8	275
15	9.9	50.3	8	181.1	8	11.6	35.9	8	26.2	N	275	11.6	35.9	8	26.2	275
27	32.5	41.4	10	211.9	9	42.2	18.4	8	47.8	N	285	42.2	18.4	8	47.8	285
28	23.9	36.3	6	212.2	10	18.0	31.7	6	18.7	Y	295	-	-	-	-	
29	16.8	37.5	7	228.6	11	11.7	44.1	8	60.0	Y	305	14.6	39.0	14	14.0	305
17	24.3	35.6	6	144.6	12	4.4	28.6	8	54.3	N	315	24.3	35.6	6	144.6	315
-	-	-	-	-	13	125.2	-23.7	7	12.6	-	327	125.2	-23.7	7	12.6	321
22	9.0	40.9	11	98.8	14	12.6	49.7	8	146.4	N	331	12.6	49.7	8	146.4	331
37	5.5	47.0	8	90.8	16	10.0	43.7	8	93.0	Y	345	10.0	43.7	8	93.0	345
38	0.1	45.3	7	127.2	17	357.4	49.1	8	70.5	Y	346	357.4	49.1	8	70.5	346
39	4.8	42.7	8	94.8	18	11.2	43.6	8	80.0	Y	346	-	-	-	-	
40	35.0	42.7	9	136.7	19	9.7	40.2	8	838.4	Y	347	-	-	-	-	
41	11.3	39.7	9	201.4	20	7.6	44.3	8	159.1	N	359	9.5	42.8	23	145.0	351
42	11.0	35.4	8	169.0	21	6.7	50.0	8	145.9	N	371	6.7	50.0	8	145.9	371
43	13.7	36.8	8	173.4	22	8.1	46.4	7	149.0	N	383	8.1	46.4	7	149.0	383
44	5.3	43.2	5	340.0	23	14.6	43.6	8	200.9	N	395	14.6	43.6	8	200.9	395
45	16.9	41.2	7	92.4	24	11.4	36.5	8	275.3	N	406	11.4	36.5	8	275.3	406
66	27.9	32.6	8	165.1	25	24.5	37.5	8	218.5	Y	418	24.5	37.5	8	218.5	418
67	13.9	38.8	5	118.2	26	6.1	46.6	7	117.3	N	430	-	-	-	-	
68	16.4	38.0	6	119.5	27	9.2	43.9	8	229.2	N	442	7.8	45.2	15	208.1	436
-	-	-	-	-	28	25.4	45.0	6	117.3	-	454	25.4	45.0	6	117.3	454
-	-	-	-	-	29	1.7	40.1	8	253.5	-	466	1.7	40.1	8	253.5	466

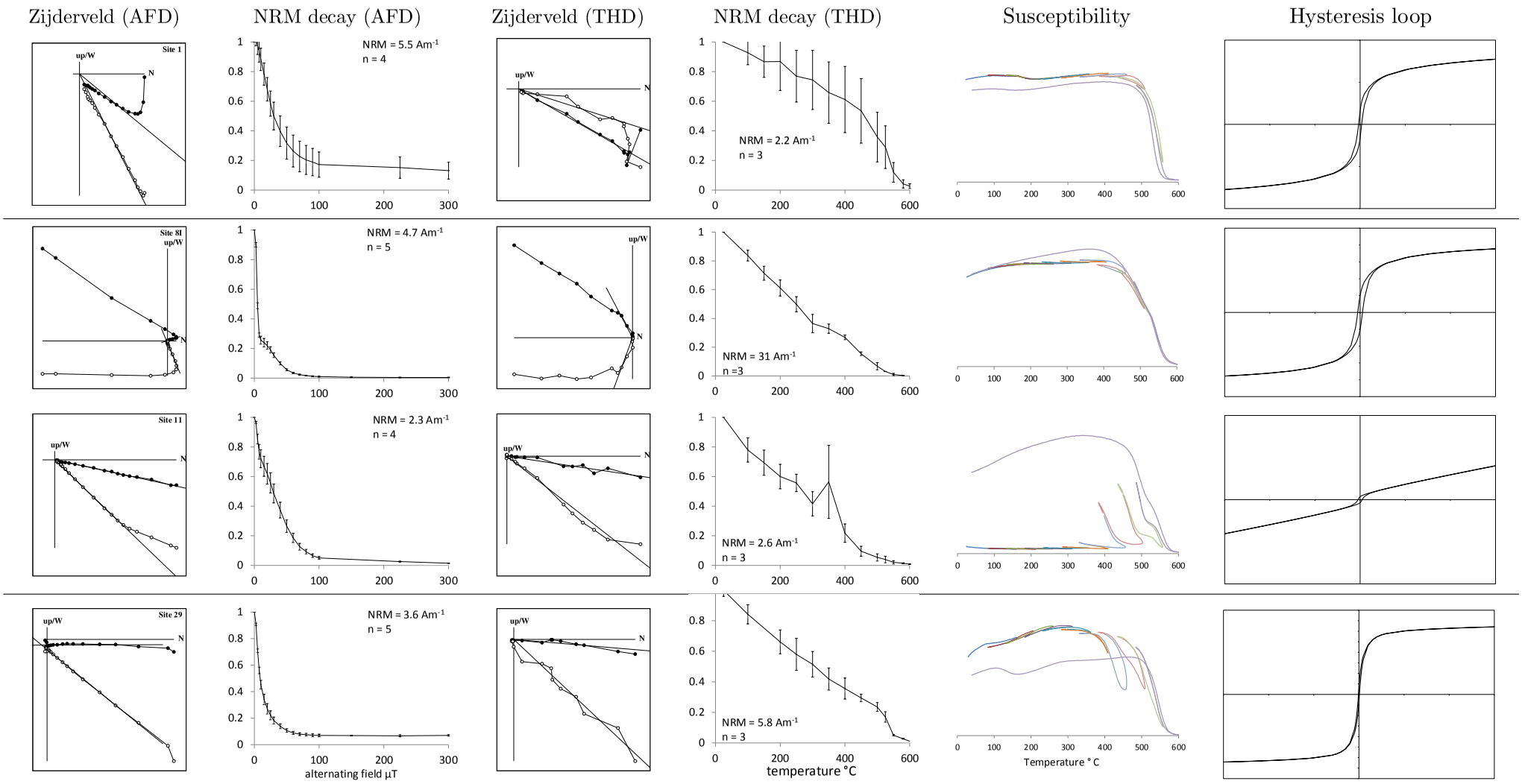
Zijderveld (AFD)
NRM decay (AFD)
Zijderveld (THD)
NRM decay (THD)
Susceptibility
Hysteresis loop
Site 1
up/W
N
NRM = 5.5 Am-1
n = 4
NRM = 2.2 Am-1
n = 3
Site 8I
NRM = 4.7 Am-1
n = 5
NRM = 31 Am-1
n =3
Site 11
NRM = 2.3 Am-1
n = 4
NRM = 2.6 Am-1
n = 3
Site 29
NRM = 3.6 Am-1
n = 5
NRM = 5.8 Am-1
n = 3
alternating field µT
temperature °C
Temperature ° C

Table 3.1: Sites from Széréméta et al. (1999) are linked to sites from this study (first column) based on paleo-directions checked for common true mean directions (CTMD). The argument for the conduction of CTMD test is based on the geographic position of the flows in both studies as seen in figure 3.2. The ages published by Széréméta et al. (1999) (errors in K-Ar generally 5 Ka) are linked to the sites in this work. Within the sites from this work a CMTD testing (McFadden & McElhinny, 1990) procedure is presented in the right part of this table. K and N values according to Fisher's statistics. (*) No K value can be calculated from N=2, 999 is adopted for further calculation.

Figure 3.3: Sites 1 (UG) 8I and 11 (MG) and 29 (LG), with for both alternating field and thermal demagnetization one representative Zijderveld diagram. For both AF and TH an averaged decay plot is shown. For sites 1, 3, 11 and 23 (appendix A), one core has been removed for the creation of the AF decay curve since the NRM of these sites was three times higher then the average.

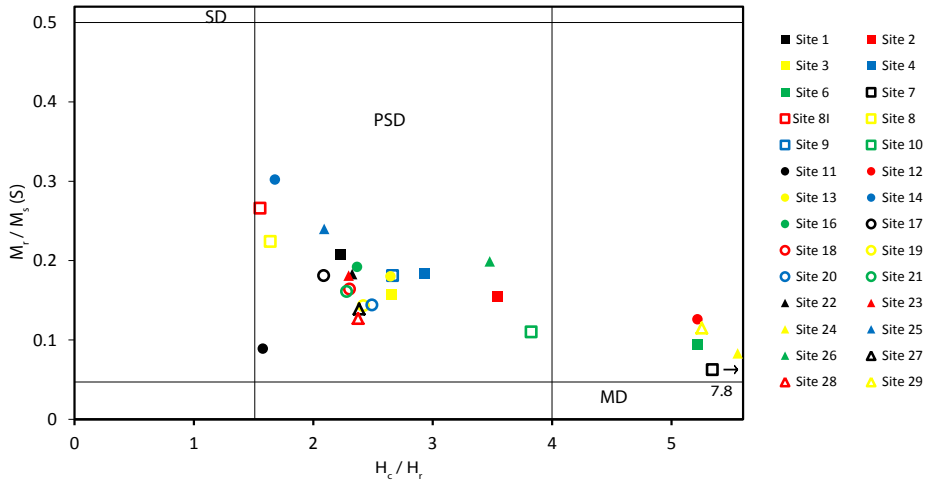

Figure 3.4: Day plot (Day et al., 1977) showing the domain state of all sites. Site 7 has a high H_c over H_r ratio and should be positioned more to the right.

3.2 Age Model

Sites 1, 7, 11, 17, 28 and 29 were prepared to be radiometrically dated using Ar/Ar dating in the new ThermoFisher Helix MC multi-collector mass spectrometer (no published data) at the VU University Amsterdam. Minerals, weathering, and other contaminations were filtered using heavy liquids, the remaining contaminants were picked by hand, so that only ground mass is left. About half a gram of this material (size 400 - 500 μm) was sent around the time of writing (beginning of November) to a nuclear reactor to be irradiated. For safety reasons the material has to be put aside for half a year. For this reason the results are not in within the scope of this project. A different provisional age model has to be created.

Széréméta et al. (1999) presents paleo-directional results from 69 lava flows some five kilometres north of the sampling location from this study (see figure 3.2). These

authors dated eight sites using K-Ar isotope dating. In order to build an age model for the sites studied here, and to get constraints on the rates of change for both the directions and intensities, sites from Széréméta et al. (1999) were linked to sites from this study. This was done by comparing the directions found in the lavas flow in both locations. The sites are linked based on stratigraphic correlation, done by following the lava flows from the aerial photographs in Google Earth (figure 3.2). The general trend here is that the lava flows have a northward dip direction which is consistent with the position of the El Golfo volcano crater (Carracedo et al., 2001; Gee et al., 2001; Longpré et al., 2011). This implies that the same lava flows, or roughly time-equivalent lava flows from Széréméta et al. (1999), can be found at a higher elevation at our location of sampling. Site 7 is of particular interest as it is found at the top the MG, and can be traced in Google Earth toward an altitude at the location of Széréméta et al. (1999) that is very close to site 14. In table 3.1 we see that site 7 and Széréméta et al. (1999)'s site 14 have a CTMD (McFadden & McElhinny (1990)). Other sites are linked based on approximate geographic position. Checks on CMTD's are shown in table 3.1. Nine of the 24 site that were tested have a CTMD, with positive result in all three defined groups. Sites 8I and 13 were not linked to other sites since they show very abnormal directions. The results from these fits are shown in figure 3.2.

With this fit, a tentative age model was created by linking the published ages to sites in this study. When a dated site was not linked the age was addressed ot the nearest site with a best estimate argument. In between linked sites ages are interpolated, assuming constant deposition rates. Sites 28 and 29 from this work fall below the section in Széréméta et al. (1999), ages were extrapolated assuming the same depositional rate of the section above. The transition from elevation to age is shown in figure 3.2.

3.3 Paleointensities

3.3.1 Thellier-Thellier Results

The Thellier-Thellier method conducted here results in 26 passed samples out of 135 measured giving it a success rate of 19%. There are results from 14 different sites, with one passed sample for sites 1, 4, 6, 18, 20 and 25. Their paleointensities will be considered in this work, with the note that they are statistically weak. Site 22 has sample 10 plotted in figure 3.5 (*). This is one of the samples that did not pass the B criteria, but exhibits very similar characteristics to sample 22-2 which did pass. Both the intensity and the error and the plot traits are very similar, where only a low temperature pTRM check causes sample 10 to fail the criteria. The other two specimens of site 22, (9 and 8) also show very coherent results and plots. These two weigh heavily on the average and the substantial difference with sample 22-2 cause the PI error (table 3.2) to increase. This is exemplary for some sites, should be taken into account when interpreting these data, and should evoke caution.

	1σ (var)(μT)	1σ (PI)(μT)	Paleointensity (μT)	N
Site 1	-	1.02	7.75	1
Site 4	-	1.21	10.04	1
Site 6	-	1.40	9.48	1
Site 7	1.44	6.12	23.76	2
Site 14	3.38	11.15	53.87	2
Site 17	2.06	0.65	22.58	2
Site 18	-	2.33	29.58	1
Site 20	-	5.17	37.29	1
Site 21	1.08	16.81	27.10	2
Site 22	0.81	13.5	27.39	3
Site 23	2.77	5.93	37.56	2
Site 25	-	2.06	60.29	1
Site 26	1.35	0.63	24.90	3
Site 29	1.63	10.12	29.89	4

Table 3.2: Results of Thellier-Thellier experiments for the 14 sites for which samples have passed the criteria by Leonhardt et al. (2004). For an N higher than 1 the paleointensities is averaged over the found intensities in figure 3.5. The standard error is calculated using two methods. For the (var) σ the variance (σ^2) of the all errors is added, square rooted and divided by N. This demands a normal distribution of the data around the correct paleointensities, which may not be the case. For that reason the PIσ is the calculated error based on the distance of the N intensities that are found. For values with an N of 1 no variance can be calculated.

The Thellier-Thellier method gives results in a large range of intensities. Paleointensities ranging from 7,75 to 60.29 μT are observed. Sites 1, 4 and 6 are very low with an intensity ($\sim$ 10 μT) less than half of the other found values, whilst sites 7 and 14 show very high paleointensities (table 3.2). When putting this into context with the current field strength at the Canary Islands (38.7 μT, IGRF-11, Finlay et al. (2010)) and published data from the PINT absolute paleointensity database (Biggin et al., 2009) we find that sites 1, 4 and 6 yield relatively low results. Even in the context of recent work published around the same latitude (e.g. Laj et al. (2011); Ravilly et al. (2001)) intensities of 10 μT and lower are very uncommon. The higher end of the found intensities are more common, with 60 μT being one of the highest intensities found in literature for the last 420 kyr (Laj & Kissel, 1999).

As mentioned before, the statistical basis for some of the sites is weak. The three most extreme values found here are all obtained from sites with only one sample passed the criteria. The difference in the accepted range of temperatures on which the linear fit is based, and the problems induced by sagging (MD behavior) result in large errors or anomalous single results. Still, the majority of the results are found between 24 - 38 μT, slightly below the current field strength, but within a plausible range.

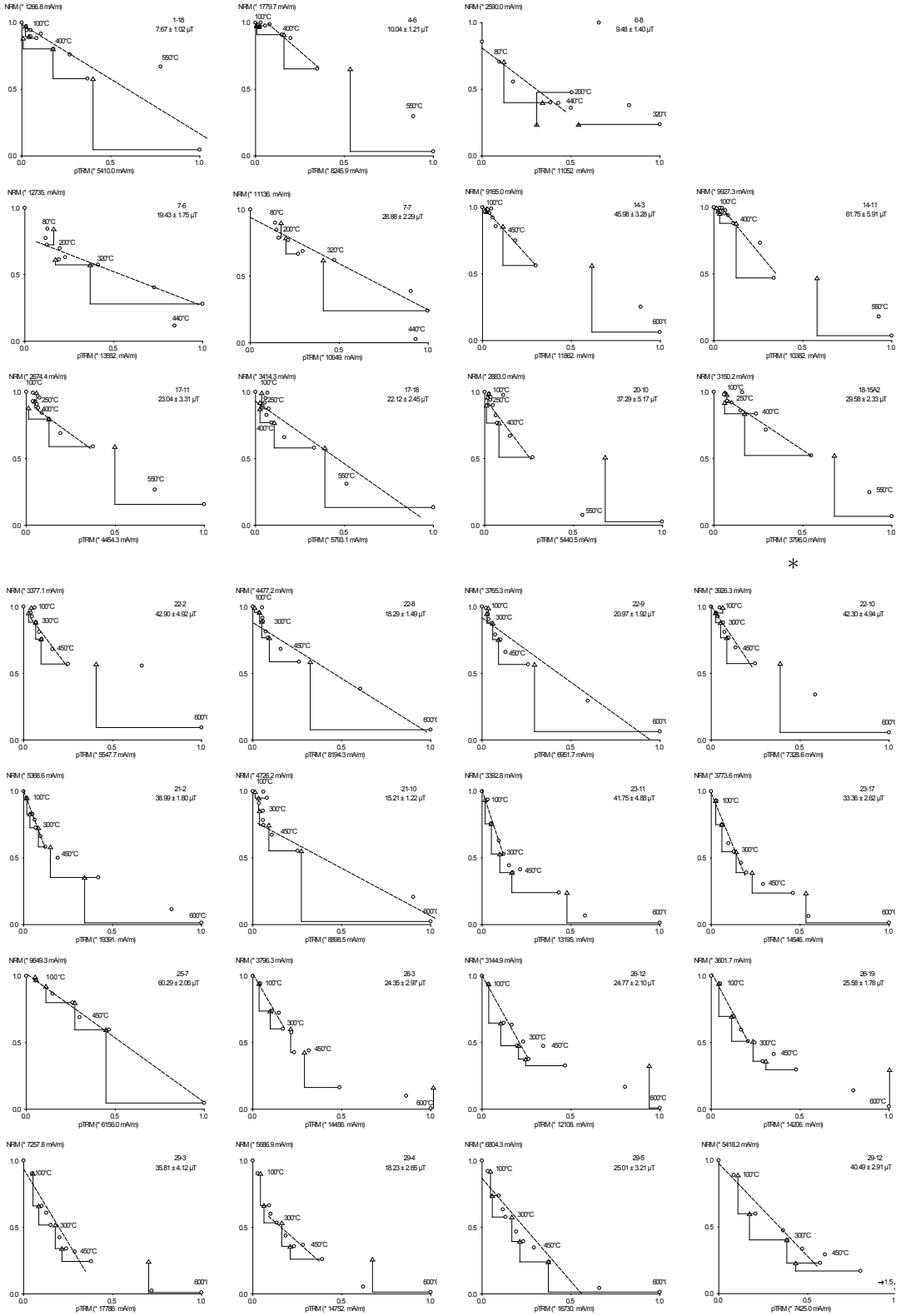
1-18
7.67 ± 1.02 µT
4-6
10.04 ± 1.21 µT
6-8
9.48 ± 1.40 µT
7-6
19.43 ± 1.75 µT
7-7
28.88 ± 2.29 µT
14-3
45.98 ± 3.28 µT
14-11
61.75 ± 5.91 µT
17-11
23.04 ± 3.31 µT
17-18
22.12 ± 2.45 µT
20-10
37.29 ± 5.17 µT
18-15A2
29.58 ± 2.33 µT
*
22-2
42.90 ± 4.92 µT
22-8
18.29 ± 1.49 µT
22-9
20.97 ± 1.92 µT
22-10
42.30 ± 4.94 µT
21-2
38.99 ± 1.80 µT
21-10
15.21 ± 1.22 µT
23-11
41.75 ± 4.88 µT
23-17
33.36 ± 2.62 µT
25-7
60.29 ± 2.06 µT
25-3
24.35 ± 2.97 µT
26-12
24.77 ± 2.10 µT
26-19
25.58 ± 1.78 µT
29-3
35.81 ± 4.12 µT
29-4
18.23 ± 2.65 µT
29-5
25.01 ± 3.21 µT
29-12
40.49 ± 2.91 µT

Figure 3.5: All accepted Thellier-Thellier Arai plots (Nagata et al., 1963) as B according to the Leonhardt et al. (2004) criteria with the exception of (*). Each plot shows site and core number, paleointensity and error in the top right corner. The NRM in can be found the top left corner, some temperature of the points are included. Site 6 (top row) passed the B criteria, but is discarded due to poor linearity and very low paleointensities. Site 22 (row 4) shows three passed samples, and one (*) that is very similar to a passed sample (see text).

3.3.2 ARM Test & Multispecimen Protocol Results

	1σ low (μT)	1σ high (μT)	Paleointenisty (μT)	$N_{initial}$	N_{used}
Site 7	18.5	39.4	31.5	10	8
Site 11	58.4	-	89.1	8	7
Site 14	8.4	42.8	27.7	9	7
Site 16	13.2	23.8	20.4	10	7
Site 17	33.5	56.6	40.9	10	8
Site 18	18.0	32.4	26.7	10	8
Site 21	10.9	29.7	22.5	8	7
Site 22	16.5	27.5	22.8	10	10
Site 25	17.1	25.3	21.5	10	5
Site 26	18.4	28.2	24.6	10	9
Site 27	14.6	39.6	29.5	10	8
Site 28	9.7	27.9	21.0	10	6

Table 3.3: The results for the multi specimen protocol give a lower and upper limit for the error on the paleointensity. The 1σ error envelope cuts the x-axis (figure 3.6) differently based on the angle of the line and the dispersion of points on both sides of the fit line. For site 11 no upper limit could be calculated since it does not cross the x-axis. The initial sample sizes ($N_{initial}$) is given and the used (N_{use}) samples after discarding outliers.

The ARM test (De Groot et al., 2012) was conducted on sites 7, 11, 12, 16 - 23, and 25 - 29. On other sites the test was not conducted when there was an overprint in the Zijderveld diagrams (Appendix A, figure 3.3), or if a site was struck by lightning. For some sites the initially chosen temperature based on the magnetic susceptibility versus temperature measurements and thermal NRM decay plots, turned out to be too high when ARM behavior was altered. For these sites (16, 19 - 21, 23, and 25 - 28) the ARM-test was repeated at a lower temperature. The sites that passed are expected to yield reliable MSP estimates. In total 75% of the sites on which it was conducted passed the ARM test. A success rate as can be easily calculated for Thellier-Thellier is more difficult for MSP, since there is a preliminary test. (For more calculations on success rate see section 4.2).

The protocol as described by Fabian & Leonhardt (2010) was conducted on all 12 sites that passed the ARM test, and results were analyzed using the a custom-made VBA macro (M.W.L. Monster, unpublished). This macro calculates all relevant

parameters, generates plots for both the DB and DSC protocol and provides several checks on the reliability of the resulting paleointensity. For sites with low alteration (<3%) the DSC protocol is plotted (figure 3.6), but when it is higher the DB protocol is preferred since it did not show alteration in the ARM-test after a single heating step. This gives a higher paleointensity, since DSC corrects for the overestimates of the paleofield caused by domain effects. The DB results can in these cases be considered as an upper limit for paleointensities.

Site 11 is the only site that did not yield reliable paleointensity results for MSP. It gives a very high result of 89.1 μT, with a very large error. The upper one standard deviation limit can not be calculated, and the lower limit differs 30 μT from the estimate. Only site 17 gives a paleointensity higher then 40 μT, and is the only site higher than the current field intensity at El Hierro (38.7 μT, IGRF-11, Finlay et al. (2010)). The results are (apart from site 11) very homogeneous, and intensities are quite low but plausible. As mentioned before, many reported intensities (using thermal Thellier-Thellier) obtained from the PINT database (Biggin et al., 2009) of similar age and at similar latitude are around 20 - 43 μT (i.e. Laj et al. (2011); Ravilly et al. (2001)).

3.3.3 Pseudo-Thellier Results

	$B_{1/2ARM}$ (μT)	PT slope	1σ	1σ\PTs	Paleointensity (μT)	N
Site 1	26.4	-0.81	0.06	0.072	20.6	4
Site 3	46.7	-0.99	0.06	0.059	22.0	5
Site 8I	30.4	-1.03	0.09	0.086	22.3	5
Site 17	39.8	-1.40	0.13	0.091	25.0	5
Site 19	28.4	-2.54	0.16	0.064	33.3	3
Site 21	38.9	-4.45	0.12	0.028	47.5	5
Site 22	48.7	-1.90	0.16	0.085	28.6	5
Site 23	24.9	-0.95	0.14	0.147	21.6	5
Site 27	28.7	-2.44	0.31	0.128	32.6	4
Site 28	29.6	-2.32	0.24	0.104	31.8	5

Table 3.4: Pseudo-Thellier results for sites that passed all tests. Showing half the field at which the full ARM is acquired (averaged over N), the pseudo-Thellier slope and correlated error. The error over the average Pseudo-Thellier slope is a test for site quality.

The Pseudo-Thellier method (De Groot et al., 2013a) was conducted on all sites except, 8, 9, 10 and 13 because their NRM is to high to be used in the robotized 2G DC SQUID magnetometer. Some sites are rejected when comparing the NRM AF demagnetization with the ARM AF demagnetization for linear behavior. Sites 6, 7, 11, 12, 18 and 24 do not show linear behavior (figure 2.6) and are discarded for further calculations. Site 14 exhibits two non-linear samples decreasing the sample

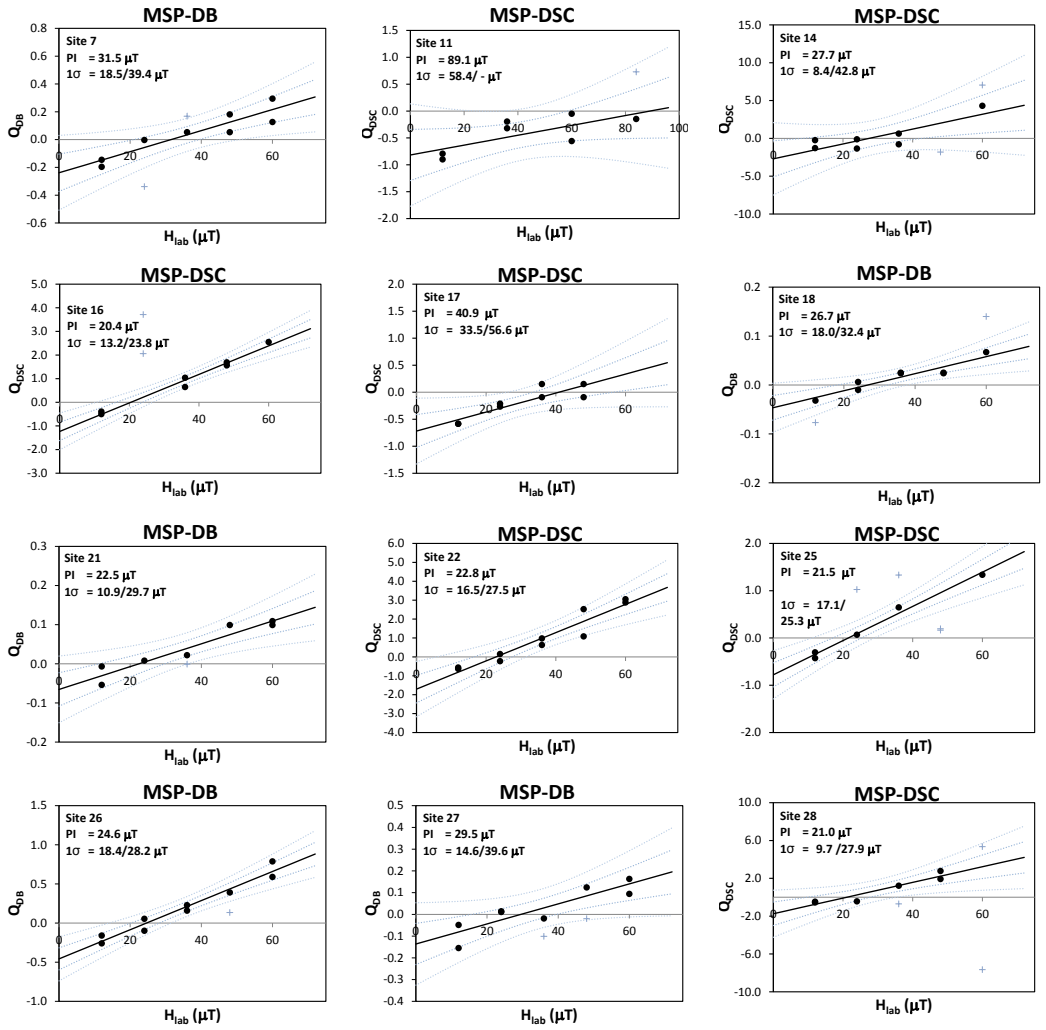

Figure 3.6: All sites that passed the ARM test (De Groot et al., 2012) were subjected to the multi-specimen protocol. For sites with an alteration lower than 3% the DSC protocol (Fabian & Leonhardt, 2010) is used and trusted, otherwise the DB protocol (Dekkers & Böhnel, 2006) was used (see text). All data points used for the linear fit are black dots, discarded point as blue crosses. Two blue dashed lines show the one and two standard deviations. These one σ x-axis cutoffs find the upper and lower shown confidence envelopes.

quantity from 5 to 3. Site 1 started with an N of 4.

The AF field strength in which half the ARM is acquired ($B_{1/2ARM}$) was determined. Sites with less than three samples in the 23-63 μT window were discarded. Sites 2, 4, 6, 7, 12, 17, 18, 20, 24, 25, 26, and 29 have three or more samples that fall, without a single exception, below the 23 μT limit. For each remaining site the standard deviation of the pseudo-Thellier slope was determined. This standard deviation can not be more than 15% of the average pseudo-Thellier slope of all measured samples. For sites 11, 14 and 16 this was the case, and they were consequently removed. The success rate for all samples measured after all selection criteria was 38%. The data for all remaining sites can be found in table 3.4.

Most of the paleointensities that were obtained from this method are within the window of realistic paleointensities that are currently expected for the Canary Islands. The present field strength for El Hierro according to the IGRF-11 model (Finlay et al., 2010) is 38.7μT. The lowest intensities of $\sim$ 20 μT are more than a third lower than the present field intensity. This is in accordance with published paleointensities found in the intensity database (Biggin et al., 2009). Intensities very similar to those found here are reported of the approximate same age and latitude using the thermal Thellier-Thellier method (Laj et al., 2011; Ravilly et al., 2001). The results in this work will be compared to other methods, and linked to the age model in section 4.

Chapter 4

Discussion

4.1 Rock-magnetic, Paleomagnetic & Age Model Discussion

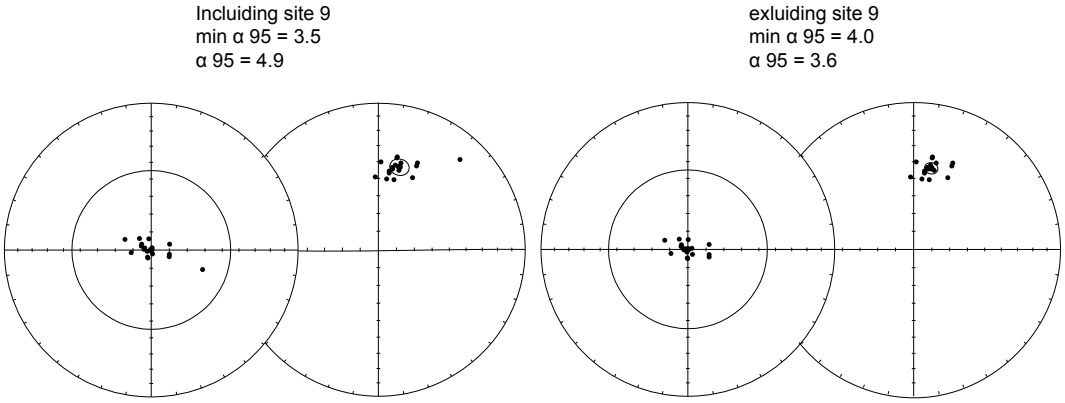

Figure 4.1: Two A95 tests (Deenen et al., 2011, 2014) that were conducted for MG and LG. Sites 8I and 13 were removed because they have been remagnetized by lightning. Site 9, considered an outlier in the remaining dataset, has a profound influence on the result (see text).

The predominantly easterly directions observed by Széréméta et al. (1999), especially in the lower El Golfo sequence have suggestively been attributed to a rotation of the island. An initial rotation of 14.2° for the El Golfo section, and a progressive 5.1° rotation for the Rift sequence. The time frame for the El Golfo section is 442 - 261 ka, or 181 kyr, giving a rotation of 7.8° per 100 kyr for the El Golfo secquence by Széréméta et al. (1999). Rapid rotations found in the oceanic micro-continents of the Easter islands (1.8° per 100 kyr) and the Galapagos micro-plate (3° - 4° per 100 kyr) (Klein et al., 2005; Schouten et al., 1993) counter claim the rate of rotation implied by Széréméta et al. (1999). Please note that there is no evidence for the Canary Island to have behaved as a micro-plate or continent.

The El Golfo section by Széréméta et al. (1999) appears roughly equivalent to the MG to LG from this study (figure 1.2), as it is stratigraphic coherent (figure 3.2) and shows an easterly deviation of 14.4°, and 12.2° for MG and LG combined, excluding site 9 (site 8I and 13 are not included). Site 9, as can be seen in figures 3.1 and 3.2,

is an outlier with an extreme easterly deviated direction and a shallow inclination. Fast loss of the NRM in AF demagnetization and an AF overprint (see appendix A) hint at a nearby lightning strike. This can also be suggested about sites 8 and 10, with the note that these sites do not produce such an extreme easterly direction as site 9, and the samples are half as magnetic as site 9.

The importance of site 9 shows when all the unique data points are subjected to the procedure described by Deenen et al. (2011, 2014) (figure 4.1) to test for a proper representation of paleosecular variation. The MG-LG part including site 9 passes the proposed A95 test, while it results in an non-representative data set for paleosecular variation when site 9 is excluded. The same procedure is conducted for both the El Golfo, Rift and the total filtered dataset of Széréméta et al. (1999). The El Golfo section has a lower A95 than required (3.1 vs. 3.3), while the Rift section has an A95 higher than required for a proper representation. The entire section by Széréméta et al. (1999) has a higher A95 than required for a properly sampled data set regarding paleosecular variation.

Using the within site scatter (Cox, 1969) of all sites in both the MG-LG and the El Golfo section compared with model G by Johnson et al. (2008), shows how the found scatter relates to the expected scatter (figure 4.2a). Both the El Golfo (Széréméta et al., 1999) and the MG-UG excluding site 9 section exhibit a scatter which is too low to properly represent paleosecular variation. Figure 4.2b shows the elongation (Tauxe & Kent, 2004) with different statistical approaches to the model. The inclusion of site 9 yields a very different result than the MG-LG and El Golfo stacks. The substantial error causes the very high elongation to be accepted for nearly all the model interpretations. When discarding site 9, it is in good agreement with the El Golfo section and it properly represents elongation.

Site 9 has a large influence on all analyses mentioned before, where the exclusion of site 9 leads to better agreement with the El Golfo section in the A95 test (Deenen et al., 2011, 2014), scatter test (Cox, 1969; Johnson et al., 2008) and the elongation test (Tauxe & Kent, 2004). In the latter one the exclusion of site 9 even leads to questionable elongation. The A95 and the within site scatter test when including site 9 leads to more representative results for paleosecular variation. The dataset of the El Golfo section is statistically stronger than MG-LG, and exhibits the same anomalous easterly directions. This combined with possible influence of lightning, justifies the assumption that site 9 is an outlier, that can be rejected. Thus here is consequently stated that the easterly directions observed are due to an unrepresentative dataset for paleosecular variation.

This is not in accordance with the conclusions by Széréméta et al. (1999), who claim that "*a period of low secular variation has occurred in the Canary Islands, in the interval between at least 442 and 261 ka.*" Added is here the remark that such an anomaly could not have gone unnoticed in the detailed insights there are on the behavior of paleosecular variation in the Brunhes chron (e.g. Langereis et al., 1997;

Lund et al., 2006; Singer, 2014).

There are three unique data point above MG (joined sites after CTMD tests, low sample density), which makes it statistically too weak for the analyses described above, and to be compared with the Rift section of Szériméta et al. (1999).

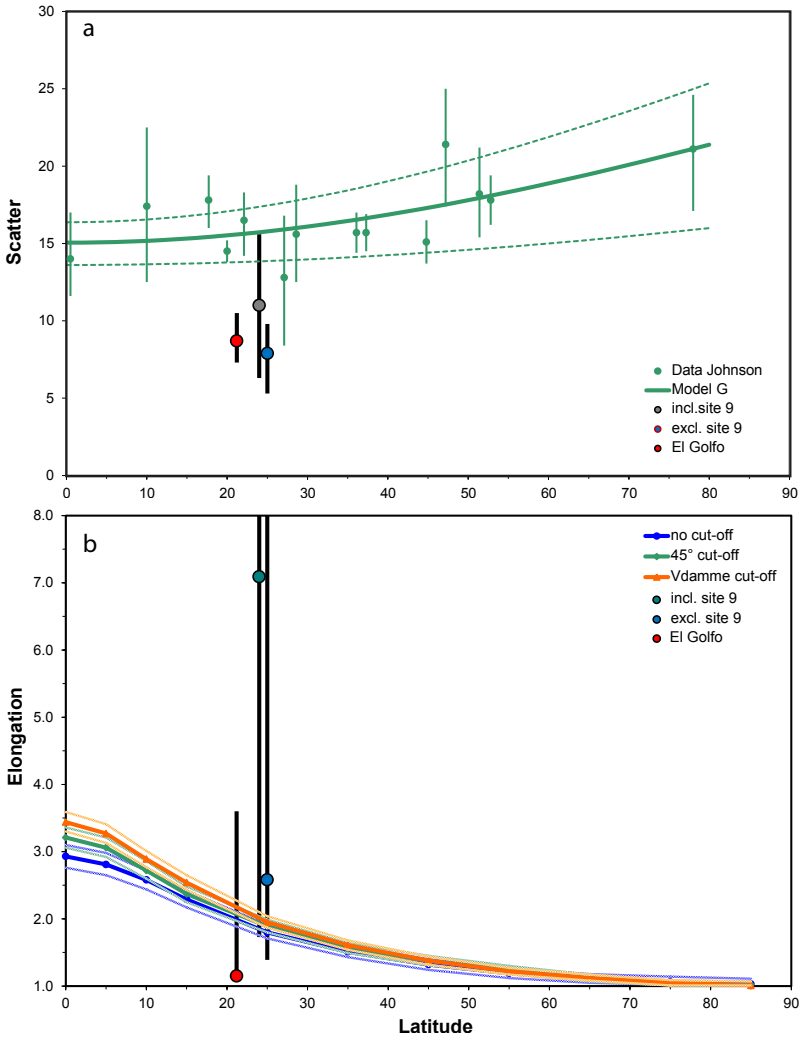

Figure 4.2: a) VGP scatter (Cox, 1969) data from the El Golfo section (Szériméta et al., 1999) according to model G by Johnson et al. (2008). The VGP scatter including and excluding site 9 from the MG and the LG combined is plotted. Both the El Golfo section and the set without site 9 exhibit less scatter than expected. When site 9 is included, the error increases and the data set falls within the window accepted by model G. b) The elongation according to Tauxe & Kent (2004), again with the El Golfo formation, and the UG and MG with and without site 9. The data excluding site 9 overlaps with the El Golfo data, adding 9 gives a significantly different result.

4.2 Paleointensity Discussion

The Thellier-Thellier method yields results for 14 different sites and is in that perspective the most successful. Of these 14 sites, five gave a result for only one out of five samples. One of these is site 6, which has one sample that passed the criteria (Leonhardt et al., 2004) even tough figure 3.5 does not shows linear behavior. This site is discarded since the pTRM checks are poor and the resulting plot is chaotic. This plot shows a problem with the criteria by Leonhardt et al. (2004), which is that some sites pass the criteria even though they do not seem reliable. In order to improve the Thellier-Thellier results, more samples should be measured to increase the statistical basis for the sites that have one accepted sample. Other improvements can be found in criteria that are not used for this work (Kissel & Laj, 2004; Selkin & Tauxe, 2000).

Several sites passed the criteria with more than one sample, but the results vary largely between the passed samples. Site 22 and 29 have high standard deviations because the temperature ranges that are chosen to plot the linear fit line on differ substantially. Because these sites exhibit domain state related sagging, the linear fit varies for different temperature ranges. This leads to varying outcomes and hence a high standard deviation (figure 3.5, table 3.2). Since the alteration temperature of these sites is high (see appendix A) it is difficult to prefer one of both temperature ranges. The MD behavior of site 22 in the Arai plot of figure 3.5 tends to indicate the lower temperature range. Site 29 shows MD behavior and sample 29-4 might be rejected due to sagging, but the high success rate for this site might strengthen the average results. Averaging the samples of sites with a big difference in intensity results per sample such as sites 22 and 29 is considered legitimated for the scope of this project. As mentioned before more measurements are suggested to improve the statistical basis and to better distinguish reliable and unreliable samples. Significant variation in the results of multiple samples of individual sites occurs more often in Thellier-Thellier (e.g. Laj & Kissel, 1999), and even in the methodologically similar (pTRM checks, progressive (de)magnetization) microwave method (Brown et al., 2009) where differences of more than 20 μT are observed.

The ARM test (De Groot et al., 2012) is conducted on sites initially selected based on their rock magnetic properties. This makes it more difficult to calculate the success rate for MSP. 75% of the sites on which the ARM test was conducted passed it. It can also be calculated from all MSP samples measured ($N_{initial}/N_{used} = 78\%$) or all sites that give a decent answer ($12/28 = 43\%$). The latter one is best comparable with the results from Thellier-Thellier, (46%) from which it differs little. One of the advantages of the ARM test and the MSP methods (Dekkers & Böhnel, 2006; Fabian & Leonhardt, 2010) combination, is the workload. The ARM test can be conducted with the robotized 2G DC SQUID magnetometer, and the sites that pass can be subjected to easily conducted MSP experiments. A second big advantage is that the chance of success can be estimated in advance, preventing work done in vain. Third,

the sample size for the passed sites is decent (N is between 5 and 10) giving it a solid statistical basis.

Site 11 exhibits high results in MSP with a paleointensity of 89μT. It shows a high upper 1σ limit, the lower limit does not intersect with the x-axis (figure 3.6) caused by the high scatter and non-linear behavior of the results per field step. The cause of these outcomes can be found in the unusual features of site 11 in the hysteresis loops (figure 3.3). The very low maximum magnetization the sample retains in zero field during hysteresis experiments shows that the samples might not yield reliable data obtained from experiments where it is subjected to an increasing field. Compared to sites in LG the magnetization that site 11 retains is one order of magnitude lower. These effect can be unnoticed since the ARM-test (De Groot et al., 2012) only checks for temperature forced alteration, and not for problems related with the uptake of an ARM as seen in hysteresis loops.

Where the alteration is higher than 3% the Dekkers & Böhnel (2006) protocol was preferred. This protocol only requires one heating step, while the repeated heating steps used in MSP-DSC can cause an even higher error. Using the DB-protocol is still preferred even though it is known that domain state problems cause a field overestimate (Fabian & Leonhardt, 2010), which is not detected in DB. Individual samples were rejected when they plot outside the 2σ window, as well as some additional samples that increase the error considerably (sites 14, 27 and 28 in figure 3.6).

A problem that occurred with MSP-DSC can cause a sample that loses little NRM at the set temperature, to return an extremely high Q_{DCS} caused by the definition of this ratio as seen in section 2.2.2. When the NRM loss is low the denominator is approximately equal to twice the NRM whilst the numerator becomes very small. Even though MSP-DSC compensates for little NRM lost, this issue remains to be solved. When these extreme samples are removed the DSC protocol yields good and reliable results. Especially sites 16, 18 22, 25, 26 and 28 show very linear behavior with very narrow error envelopes. The remaining sites are accepted with a slightly higher errors.

Work done on historical lavas has shown that MSP-DSC gives correct estimates of the paleofield (De Groot et al., 2013a), while in other studies underestimates are found (De Groot et al., 2013b). Causes for these inconsistencies can be found in the cooling rate and the chosen temperature for the experiment (De Groot et al., 2013b; Muxworthy et al., 2011; Muxworthy & Taylor, 2011) and irreversible domain state problems, even at low temperature MSP experiments (De Groot et al., 2014b; Muxworthy & Heslop, 2011). Domain state changes and thermal alteration generally leads to an enhanced uptake of a pTRM and, consequently, an underestimate of the paleofield for both Thellier-Thellier and MSP experiments. The checks, tests, and selection criteria mentioned before give constraints on these problems, but these are still the main issues to be resolved for thermal paleointensity research.

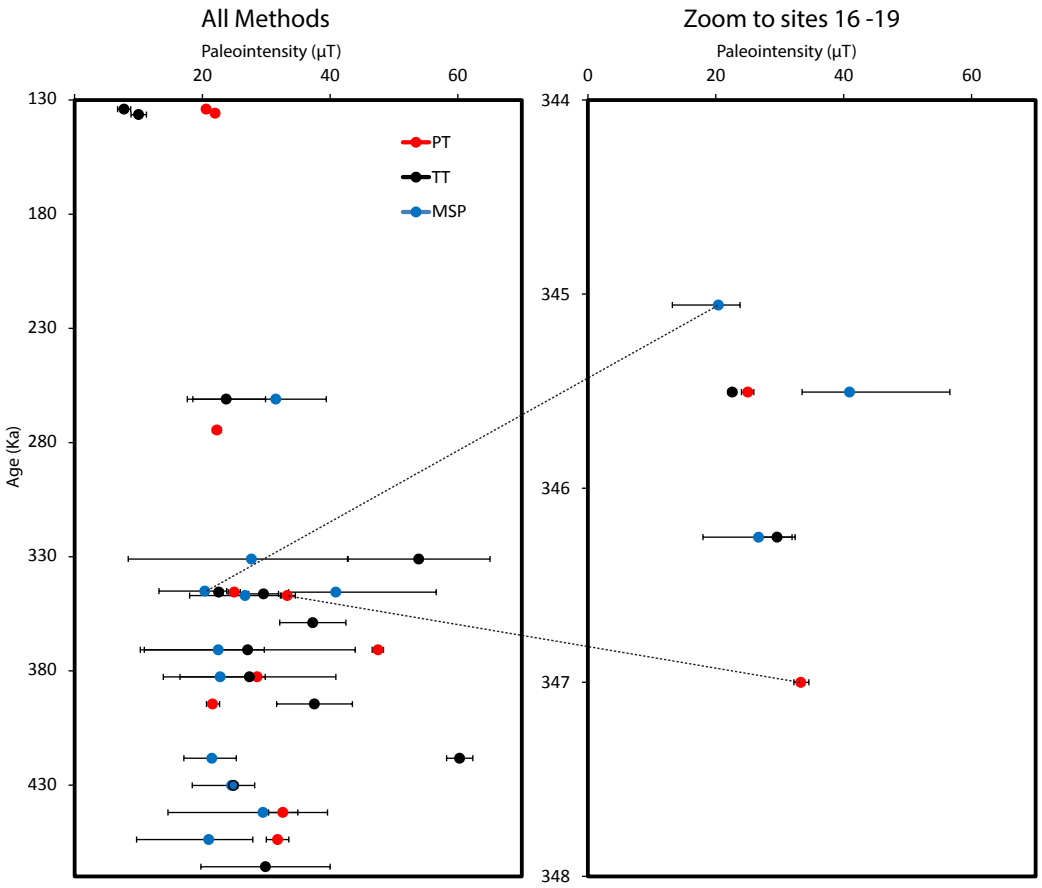

Figure 4.3: All results of all applied paleointensity methods of all sites that are considered reliable are linked to the age model (see section 3.2 and 3.3). Note that at 430 ka a TT and MSP result overlap, the TT result is shown in as a black circle. The age model is very compressed around sites 16 - 19; a zoomed plot shows some consensus for all methods in these sites.

The Pseudo-Thellier method yields results for 10 out of the 24 sites on which it is conducted with low paleointensities of 21 - 33 μT. The only exception is site 21 with an intensity of 48 μT. Even though the results are generally low, they are often higher than the results of the thermal methods (figure 4.3), which is not in accordance with earlier work done one Pseudo-Thellier (De Groot et al., 2013a, 2014a).

There is little work done using the empirical Pseudo-Thellier method; all the work that is reported is conducted on historic Hawaiian lavas (De Groot et al., 2013a, 2014a). This in contrast to the Thellier-Thellier method, which has a long history and has seen improvements and additions since the first proposal by Thellier & Thellier (1959). To a lesser extend we can argue more has to be done using both the MSP protocols. Even though it is a recent method (Dekkers & Böhnel, 2006; Fabian & Leonhardt, 2010), the basis for it is increasing. Another difference between the three

	Thellier-Thellier intensity μT	MSP intensity μT	Pseudo-Thellier intensity μT	Age (ka)
Site 1	7.8	-	20.6	134
Site 3	-	-	22.0	136
Site 4	10.0	-	-	136
Site 7	23.8	31.5	-	261
Site 8I	-	-	22.3	275
Site 14	53.9	27.7	-	331
Site 16	-	20.4	-	345
Site 17	22.6	40.9	25.0	346
Site 18	29.9	26.7	-	346
Site 19	-	-	33.3	347
Site 20	37.3	-	-	359
Site 21	27.1	22.5	47.5	371
Site 22	27.4	22.8	28.6	383
Site 23	37.6	-	21.6	395
Site 25	60.3	21.5	-	418
Site 26	24.9	24.6	-	430
Site 27	-	29.5	32.6	442
Site 28	-	21.0	31.8	454
Site 29	29.9	-	-	466

Table 4.1: The paleointensity results that have an overlapping error envelope shown in light green (figure 4.3). The Pseudo-Thellier results have little overlap with the other data, but this is also due to the fact that the size of the error is a selection criterion (section 2.2.3). Nineteen sites yielded at least one result, twelve al least two and sites 22 and 17 are the only sites that have results for all three methods. For the 12 sites that have at least two results we see 7 that overlap. Site 22 shows an overlap for all three methods.

techniques is the fact that MSP and Thellier-Thellier are thermal intensity methods. This is generally considered a better analogue for the recording of the magnetic signal in outflowing lavas. Even so, the Pseudo-Thellier method looks promising. The biggest issue is thus the lack of robust and quantitative multi-protocol data and thorough testing of the protocol on lavas from a wide array of ages and localities. The results in this work can be seen as an attempt to address this issue.

The paleointensity data for all methods can be divided in two groups based on the quantity of data. This is Lower Group (LG), and all the sites that are younger. For all the younger sites than LG there are 9 paleointensity results in 215 kyr (figure 4.3, table 4.1), for LG there are 24 found in 135 kyr. For this reason it is not prudent to discuss trends in this younger time frame. Nonetheless, some notes on it can be made.

The low Thellier-Thellier ($\sim$ 10 μT) results, which differ from the Pseudo-Thellier ($\sim$ 20 μT) results for the UG around 130 ka are anomalous for lavas of this age and similar locations (e.g. Biggin et al., 2009; Laj et al., 2011). Attributing these low results to excursions (Langereis et al., 1997; Lund et al., 2006) is difficult, since the directions do not support this (appendix B). The MG and the stratigraphic island site 14 yielded 5 intensity results, sites 7 and 14 have results from two methods that can be considered equivalent (figure 4.1). Even tough the Thellier-Thellier and MSP paleointensities for these sites differ substantially, the large error envelopes in both methods cause them to overlap. For this part of the section the intensities are perdominantly below 25 μT. With the exception of the Thellier-Thellier results for site 14, all intensities are below the current field value for El Hierro (37.1 μT, IGRF-11 Finlay et al., 2010). MSP results for site 7 are just above 31 μT, while the rest is below 25 μT. This may suggest that in the period 345 - 130 ka there were several moments on which the paleointensity was at least $\sim$ 15 μT lower than todays values. Note that, as mentioned before, the data density in this part of the section is not considered high enough to conclude more than the previous statement.

The oldest LG flows (29-27) show consistent results, with the exception of MSP for site 28 (21 μT). All three methods yield intensities of $\sim$ 30 μT with a very good MSP and Pseudo-Thellier overlap for site 27 (table 4.1). Site 26 shows the best coherency in methodology, Thellier-Thellier and MSP show a very consistently 25 μT, which is 5 μT lower than the older segment.

Sites 25 - 21 yield two results higher than the trend we observe. Thellier-Thellier for site 25 gives 60 μT for site 23 it shows 38 μT. Especially the Thellier-Thellier result for site 25 is anomalous, being the highest accepted intensity found. The intensity of 38 μT for site 23 is high compared to Pseudo-Thellier and the surrounding data. Since it is based on two Thellier-Thellier results, and since it is very comparable with the current field strength it can not be ignored. The discrepancy between Pseudo-Thellier and Thellier-Thellier remains, but considering the given arguments regarding the long history of Thellier-Thellier compared to the recent Pseudo-Thellier method the latter one is considered to be more credible to date. For sites 22 and 21 all methods (except Pseudo-Thellier for site 21 which appears to be anomalous) are in fair agreement, a paleointensity of $\sim$ 25 μT is here probable.

The youngest part of LG (359 - 345 ka) has a high data density in only 14 kyr. This is due to the compression of the age model in this time window (figures 3.2 and 4.3). The low intensities found for sites 22 and 21 increase for sites 20 and 19, with the note these results are based on one method. An increase of $\sim$ 10 μT for site 20 relative to site 21 is observed, with only one accepted sample for Thellier-Thellier. This small peak falls back to the trend of low intensities: $\sim$ 28 μT for site 18, $\sim$ 23 μT for site 17 and even 20 μT for site 16. The only exception here is the MSP result for site 17, which the highest accepted value for MSP and does not fit the trend.

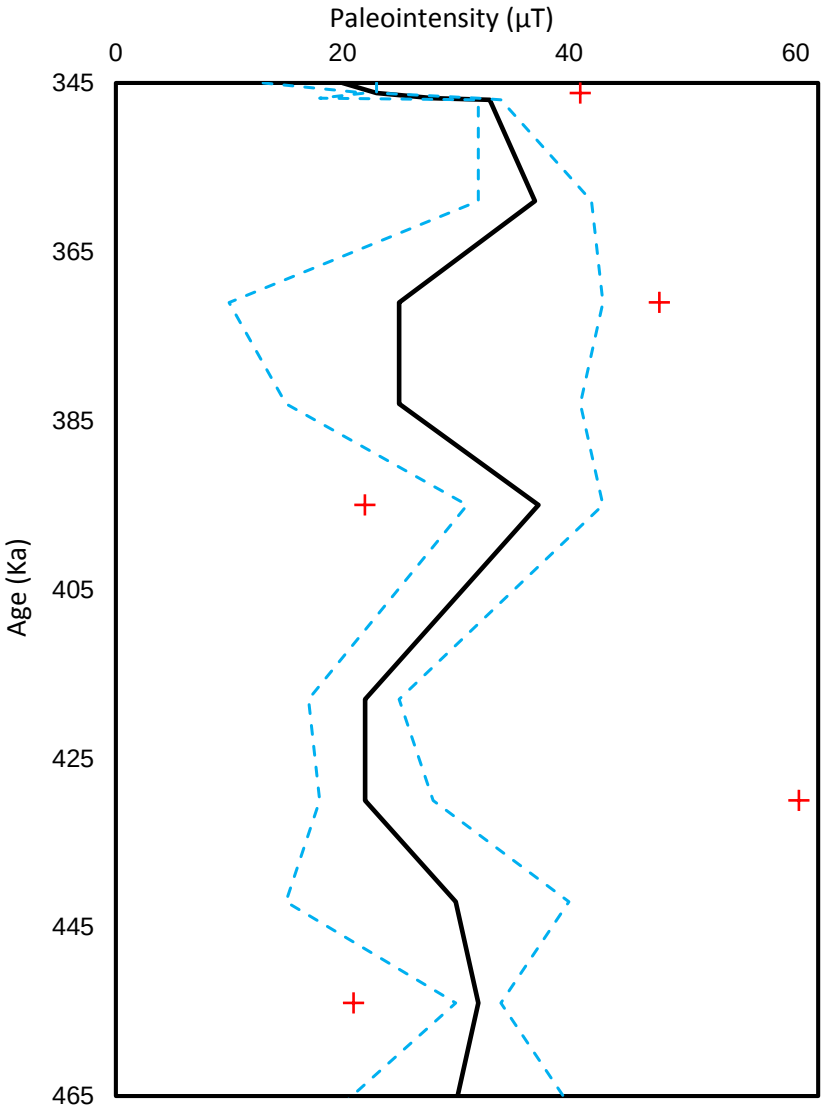

Figure 4.4: the trend as discussed (see text) for LG, hence a filtered and averaged version of figure 4.3. Red crosses represent all data points that are not considered. Blue dashed lines are the confidence intervals based on the highest error in case of multiple methods, as seen in section 3.3. Note that for Pseudo-Thellier the error is small, causing other methods to fall out the confidence window at 454 and. At this point the trend is chosen to follow the Pseudo-Thellier, and not MSP in order to fit an more continuous trend. This can be chosen otherwise.

When considering this trend for LG, from 465 to 345 ka, the intensities are lower than the current field intensity (figure 4.4). Of the 25 data points, three are considered high in this context, leaving 22 paleointensities between 20 and 37 μT, all of which are below or equal to the current intensity of 37.1 μT (IGRF-11, Finlay et al., 2010).

Chapter 5

Conclusion

This work demonstrates that MG and LG are age equivalent with the El Golfo section by Széréméta et al. (1999), supported by the stratigraphic coherency and the predominant eastward paleodirections. The consistently deviating directions found from 466 - 261 ka are attributed to an unrepresentative data set to properly depict paleosecular variation (Deenen et al., 2011, 2014). The within site scatter (Cox, 1969) for both the MG-LG and the El Golfo section are lower than might be expected for El Hierro, further strengthening this inference. Suggested here is to strengthen the available data regarding the paleodirections in the mentioned time frame on other Canary Islands, since El Hierro does not properly depict paleosecular variation.

The paleointensity work is done using three methods. The Thellier-Thellier method knows a long history of improvements (e.g. Aitken et al., 1988; Coe et al., 1978; Leonhardt et al., 2004; Riisager & Riisager, 2001; Thellier & Thellier, 1959) and has proven itself as a useful method (e.g. De Groot et al., 2013a; Laj & Kissel, 1999; Ravilly et al., 2001). The recent multi-specimen parallel differential pTRM method (Dekkers & Böhnel, 2006), and the expanded domain state corrected protocol (Fabian & Leonhardt, 2010) in combination with the ARM-test (De Groot et al., 2012) dramatically reduces the workload compared to Thellier-Thellier. The theory is robust and rich in potential, although the data quantity for the method has to be increased for it to be fully tested. The very recent and labor extensive Pseudo-Thellier approach (De Groot et al., 2013a) is empirically based on, and only applied to, historic Hawaiian lavas. It needs more work on a wide array of ages and localities to be fully considered reliable. This work attempts to do so.

The consensus with these methods is good. Ten of the nineteen sites that have an accepted paleointensity result have this for at least two methods, two of the nineteen have this for all three. Of the ten sites with two results, six are in good consensus. One of the sites with all three methods accepted shows good cohesion (table 4.1).

The paleointensity results are divided into groups, the LG (466 - 345 ka) with 25 data points and all sites that are younger (331 - 134 ka), showing only 9. With only one anomalously high paleointensity (54 μT), and one result of 31 μT the intensities in the young group are considered low compared to the present field intensity of 37

μT (Finlay et al., 2010). The limited data in this section leads to the conservative remark that from 331 - 134 ka there were several moments on which the paleointensity was at least $\sim$ 15 μT lower than it is today. LG spans less time, but shows more paleointensity results, making it possible to discuss trends (figure 4.4). From 465 - 445 ka the intensity was $\sim$ 30 μT going down to 25 - 21 μT at 240 - 418 ka. An increase is observed at 395 ka (38 μT) before a period of intensities again around 25 μT is seen ending at an increase to 37 μT around 359 ka. A final period of decrease in the paleointensity to a value of 20 μT is observed at 345 ka. Five of the 25 intensities in LG are not considered since the discrepancy between the three methods was too large. The motivation to decide which result to accept was primary based on the robustness of the method and secondary on the paleointensity trend. More work on El Hierro should be considered, since it is suitable for intensity purposes.

Chapter 6

Acknowledgements

During the stay on El Hierro help was offered to overcome unforeseen difficulties by the local tourist office, especially the help by Cristina Ferro is acknowledged. Assistance in the framework for this layout, and the availability for problem solving by Bram Schermers and Tom Steinbusch was appreciated. For the creation of the stratigraphic column in figure 1.2 substantial assistance by Léon Leeflang is acknowledged. Help in the field by Annemarieke Béguin was much appreciated. Help in the field and assistance for the VSM by Lennart de Groot was very useful. Assistance with the use of, and acquiring some technical insight in many of Fort Hoofddijks measurement equipment by Maxim Krasnoperov is acknowledged. Many very helpful and educative talks with the always patient Mark Dekkers are especially acknowledged. For tips and assistance on the directional chapters, and for availability to be the second supervisor is Cor Langereis thanked. First supervisor Marilyn Monster is thanked for all the advise, help and the invitation to work on this project. Her style of guidance suits this author very well, and made the duration of the project very enjoyable.

Chapter A

Rock-magnetic Appendix

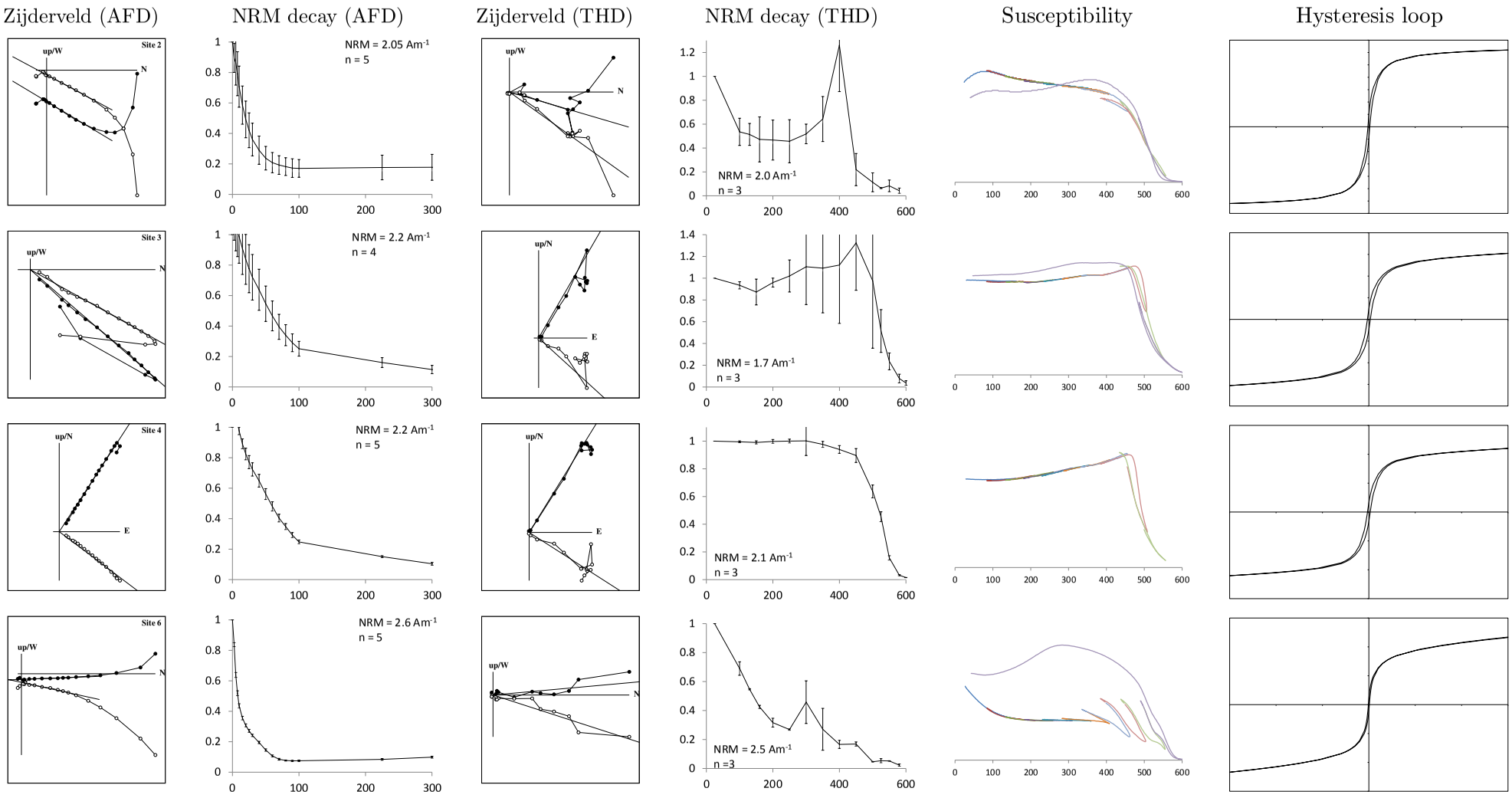
Zijderveld (AFD)
NRM decay (AFD)
Zijderveld (THD)
NRM decay (THD)
Susceptibility
Hysteresis loop
Site 2
up/W
N
NRM = 2.05 Am-1
n = 5
NRM = 2.0 Am-1
n = 3
Site 3
up/W
N
NRM = 2.2 Am-1
n = 4
up/N
E
NRM = 1.7 Am-1
n = 3
Site 4
up/N
E
NRM = 2.2 Am-1
n = 5
NRM = 2.1 Am-1
n = 3
Site 6
up/W
N
NRM = 2.6 Am-1
n = 5
NRM = 2.5 Am-1
n =3

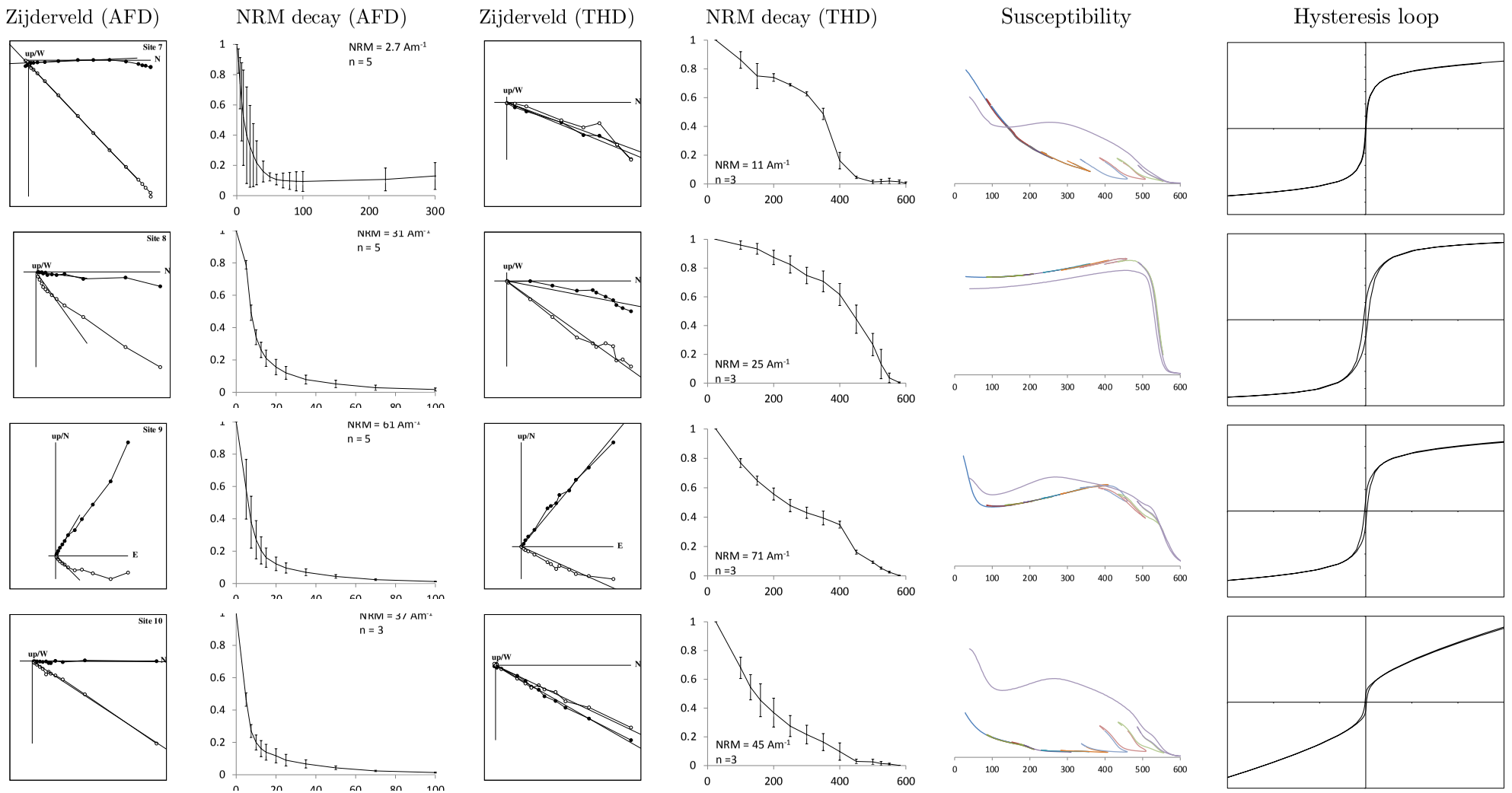
Zijderveld (AFD)
NRM decay (AFD)
Zijderveld (THD)
NRM decay (THD)
Susceptibility
Hysteresis loop
Site 7
up/W
N
NRM = 2.7 Am-1
n = 5
NRM = 11 Am-1
n =3
Site 8
NRM = 31 Am-1
n = 5
NRM = 25 Am-1
n =3
Site 9
up/N
E
NRM = 61 Am-1
n = 5
NRM = 71 Am-1
n =3
Site 10
NRM = 37 Am-1
n = 3
NRM = 45 Am-1
n =3

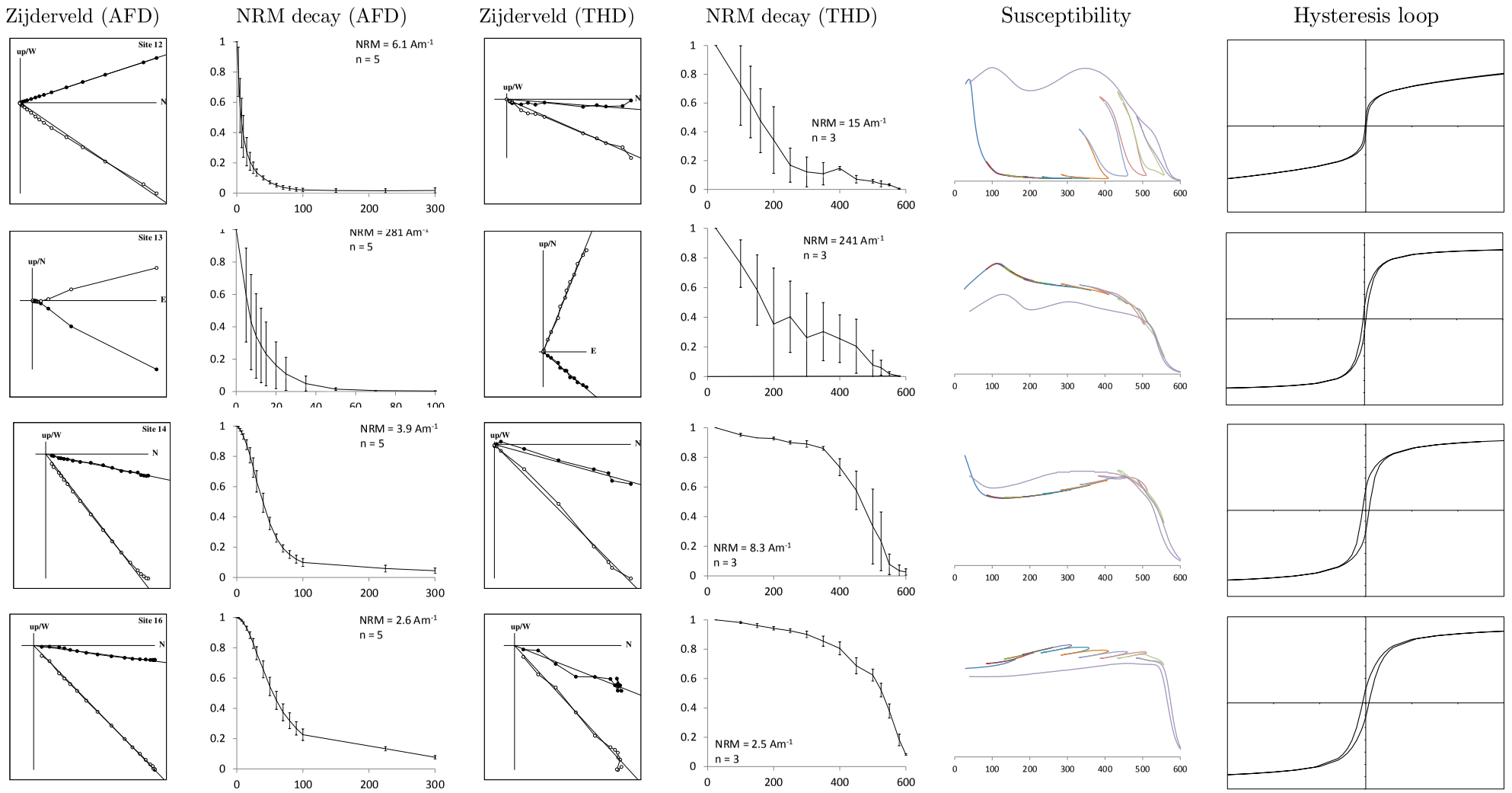
Zijderveld (AFD)
NRM decay (AFD)
Zijderveld (THD)
NRM decay (THD)
Susceptibility
Hysteresis loop
Site 12
up/W
N
NRM = 6.1 Am-1
n = 5
NRM = 15 Am-1
n = 3
Site 13
up/N
E
NRM = 281 Am-1
n = 5
NRM = 241 Am-1
n = 3
Site 14
NRM = 3.9 Am-1
n = 5
NRM = 8.3 Am-1
n = 3
Site 16
NRM = 2.6 Am-1
n = 5
NRM = 2.5 Am-1
n = 3

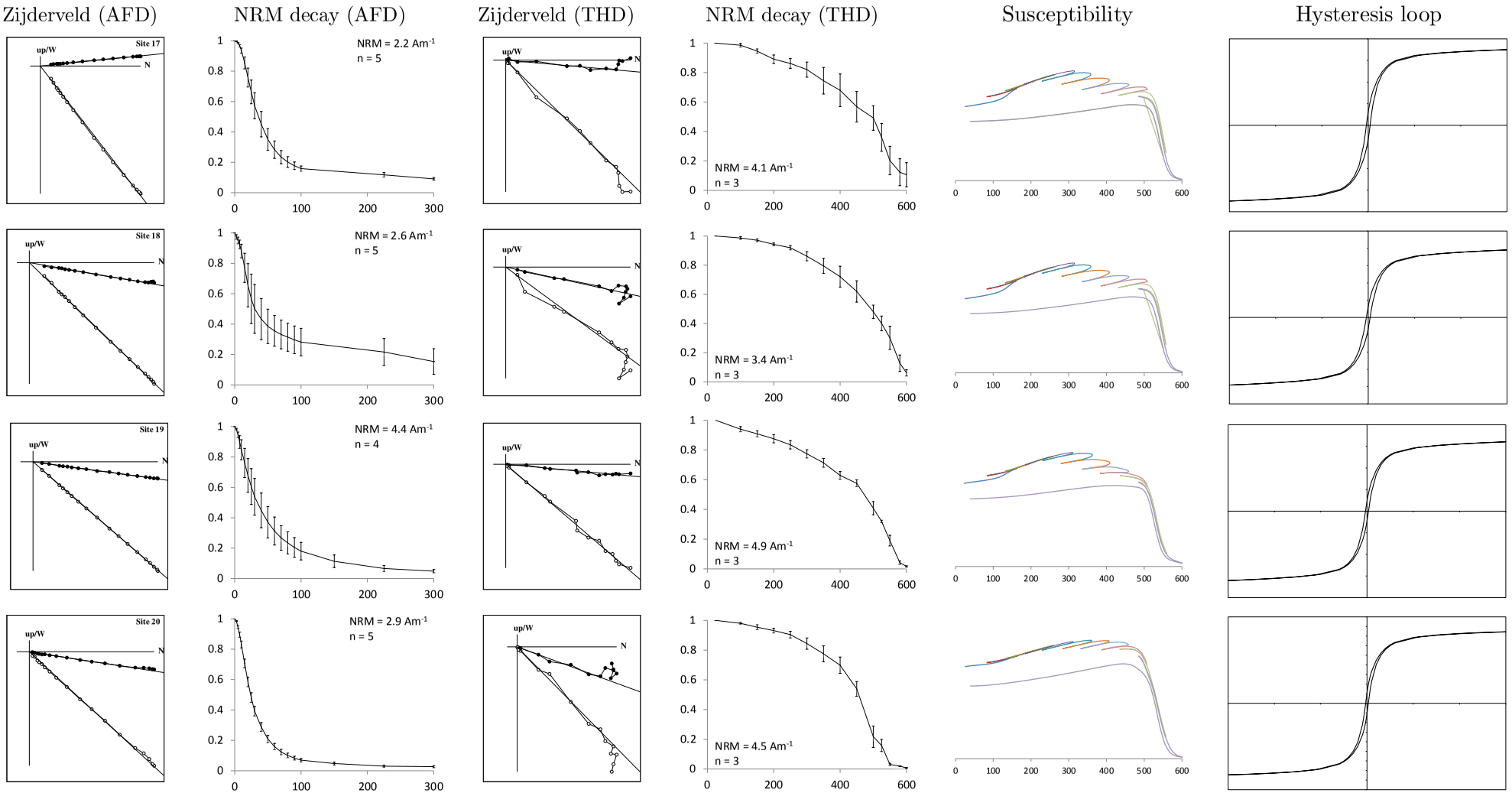
Zijderveld (AFD)
NRM decay (AFD)
Zijderveld (THD)
NRM decay (THD)
Susceptibility
Hysteresis loop
Site 17
up/W
N
NRM = 2.2 Am-1
n = 5
NRM = 4.1 Am-1
n = 3
Site 18
NRM = 2.6 Am-1
n = 5
NRM = 3.4 Am-1
n = 3
Site 19
NRM = 4.4 Am-1
n = 4
NRM = 4.9 Am-1
n = 3
Site 20
NRM = 2.9 Am-1
n = 5
NRM = 4.5 Am-1
n = 3

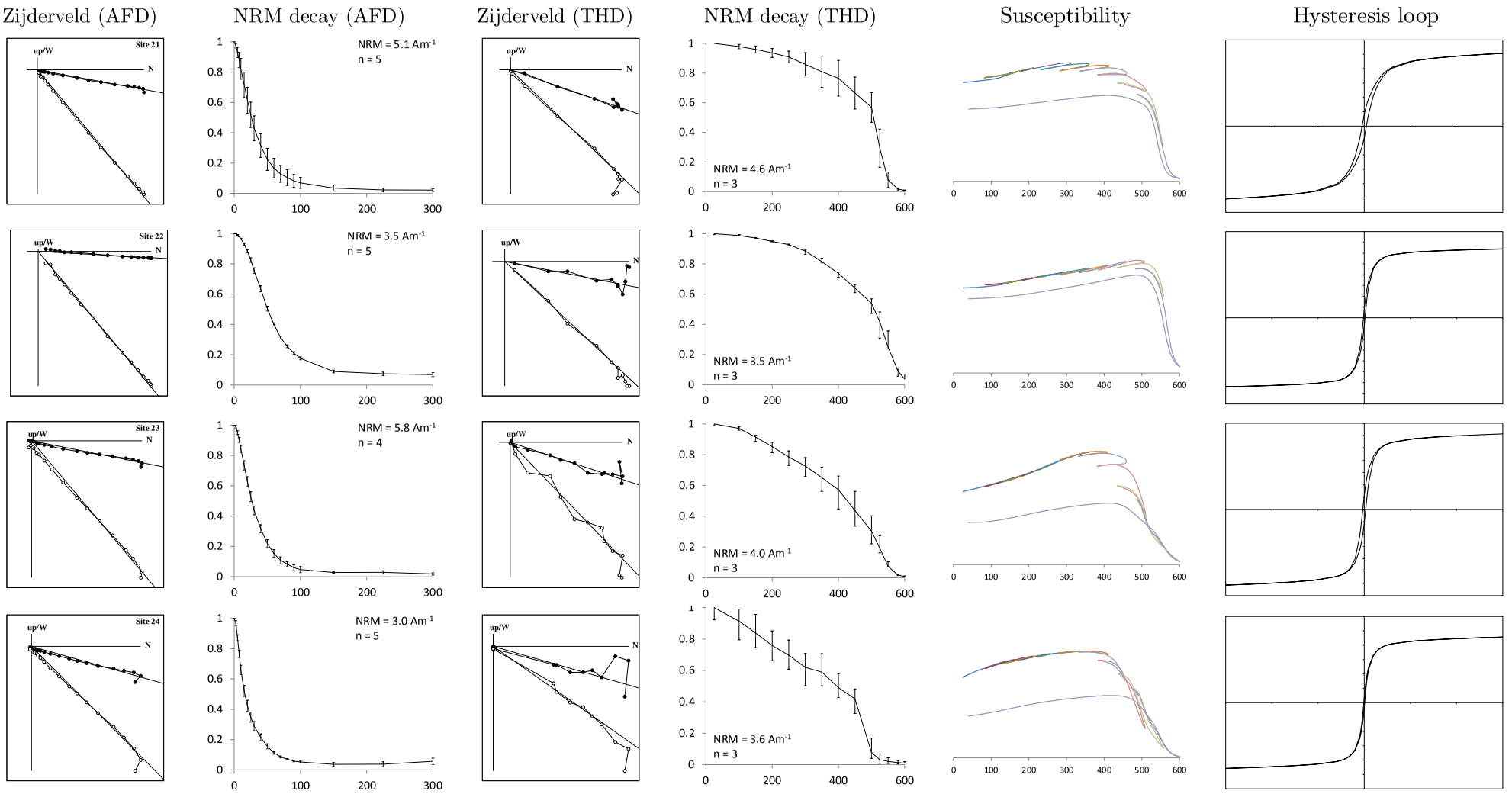
Zijderveld (AFD)
NRM decay (AFD)
Zijderveld (THD)
NRM decay (THD)
Susceptibility
Hysteresis loop
Site 21
NRM = 5.1 Am-1
n = 5
NRM = 4.6 Am-1
n = 3
Site 22
NRM = 3.5 Am-1
n = 5
NRM = 3.5 Am-1
n = 3
Site 23
NRM = 5.8 Am-1
n = 4
NRM = 4.0 Am-1
n = 3
Site 24
NRM = 3.0 Am-1
n = 5
NRM = 3.6 Am-1
n = 3
up/W
N

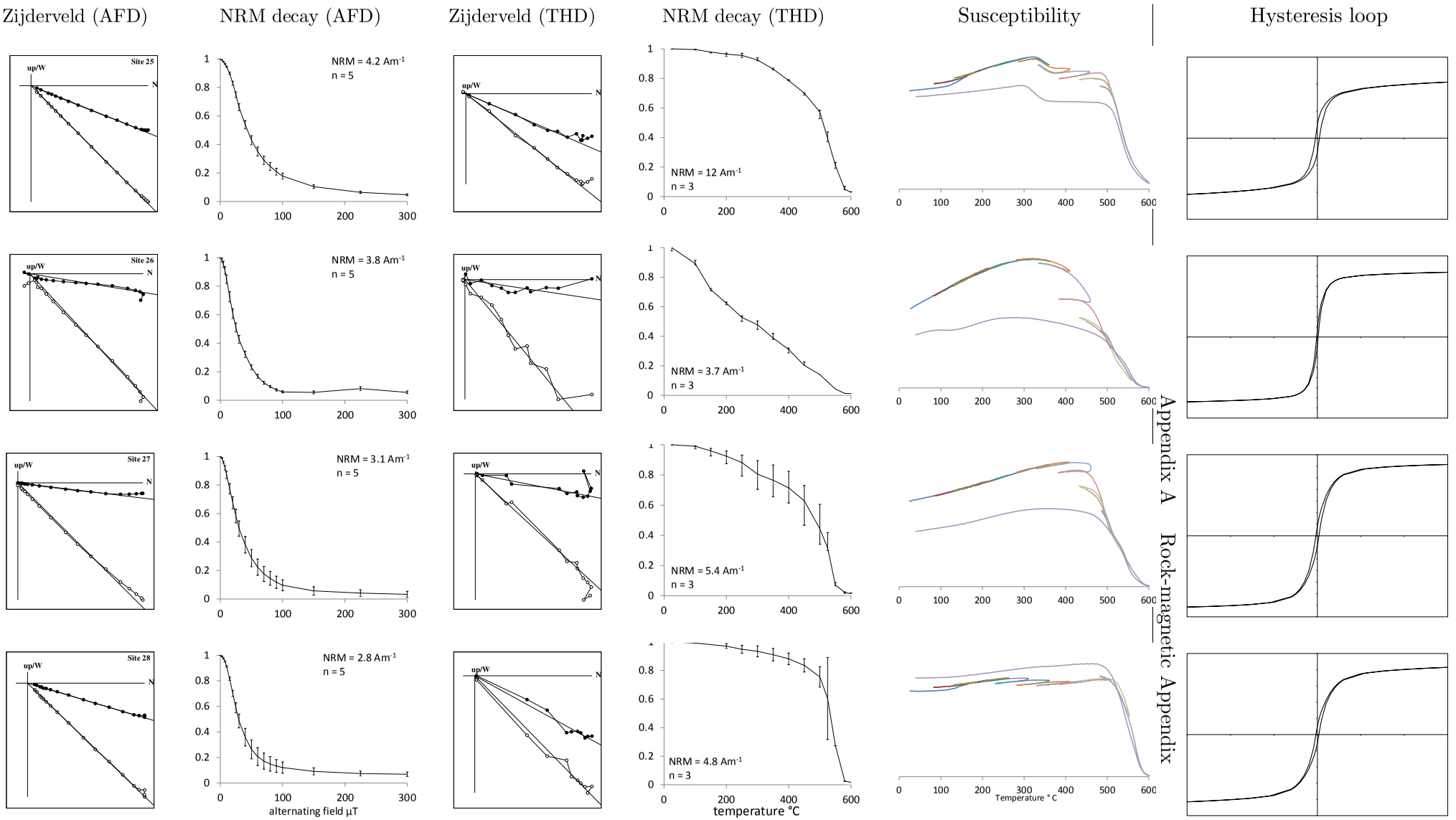
Zijderveld (AFD)
NRM decay (AFD)
Zijderveld (THD)
NRM decay (THD)
Susceptibility
Hysteresis loop
Site 25
Site 26
Site 27
Site 28
up/W
N
NRM = 4.2 Am-1
n = 5
NRM = 3.8 Am-1
n = 5
NRM = 3.1 Am-1
n = 5
NRM = 2.8 Am-1
n = 5
NRM = 12 Am-1
n = 3
NRM = 3.7 Am-1
n = 3
NRM = 5.4 Am-1
n = 3
NRM = 4.8 Am-1
n = 3
alternating field µT
temperature °C
Temperature ° C

Chapter B

Paleodirectional Appendix

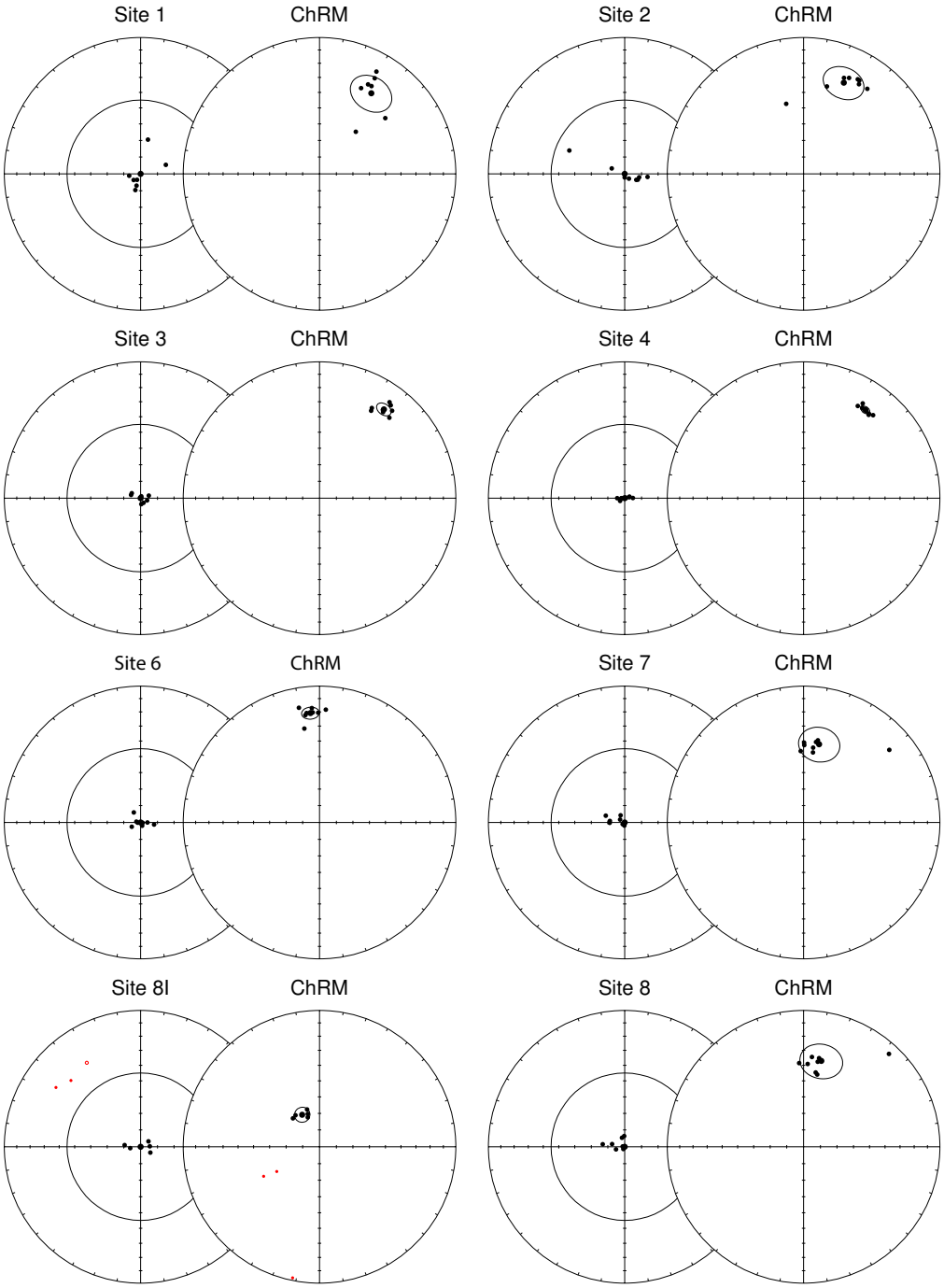
Site 1
ChRM
Site 2
ChRM
Site 3
ChRM
Site 4
ChRM
Site 6
ChRM
Site 7
ChRM
Site 8I
ChRM
Site 8
ChRM

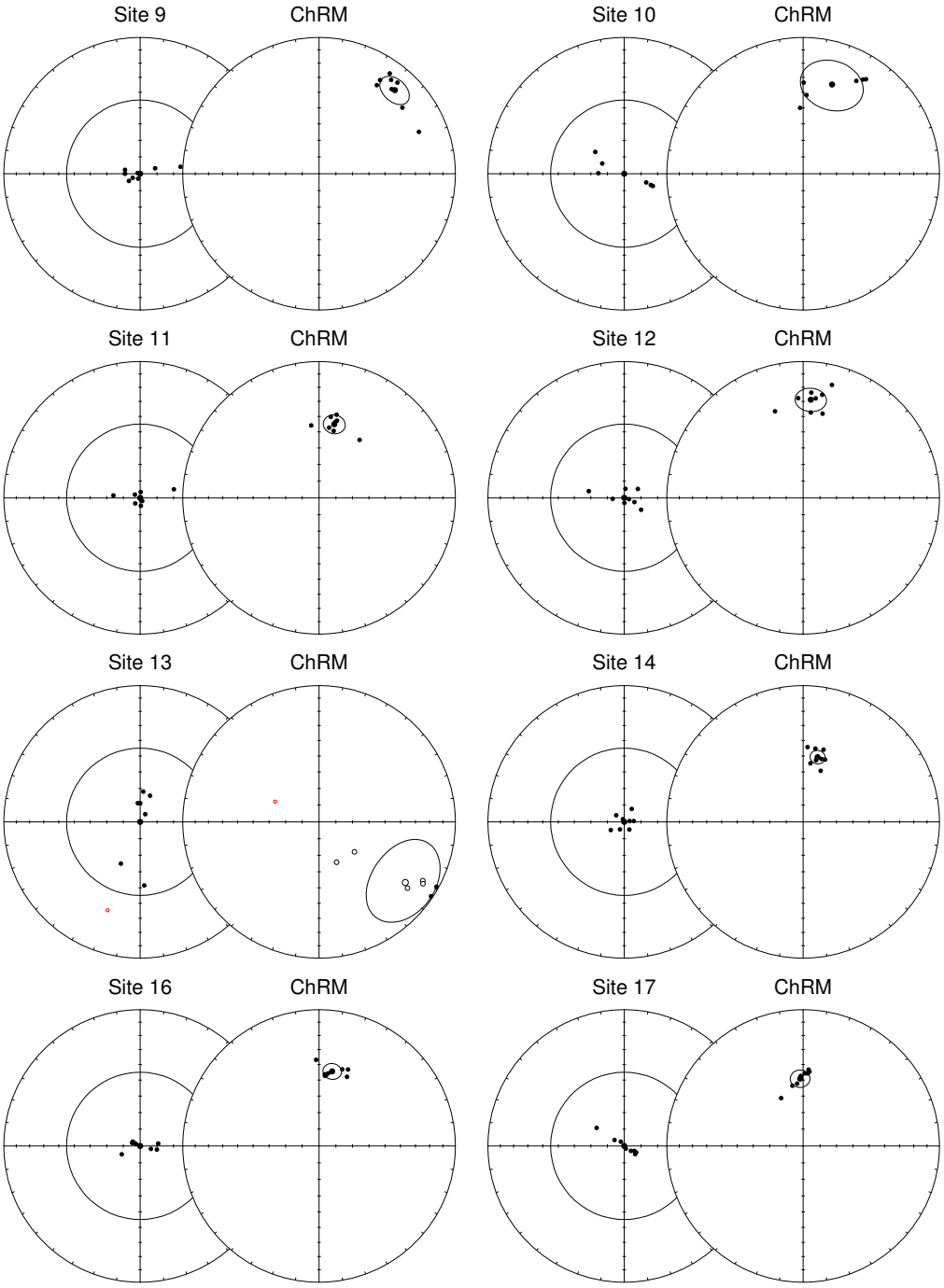
Site 9
ChRM
Site 10
ChRM
Site 11
ChRM
Site 12
ChRM
Site 13
ChRM
Site 14
ChRM
Site 16
ChRM
Site 17
ChRM

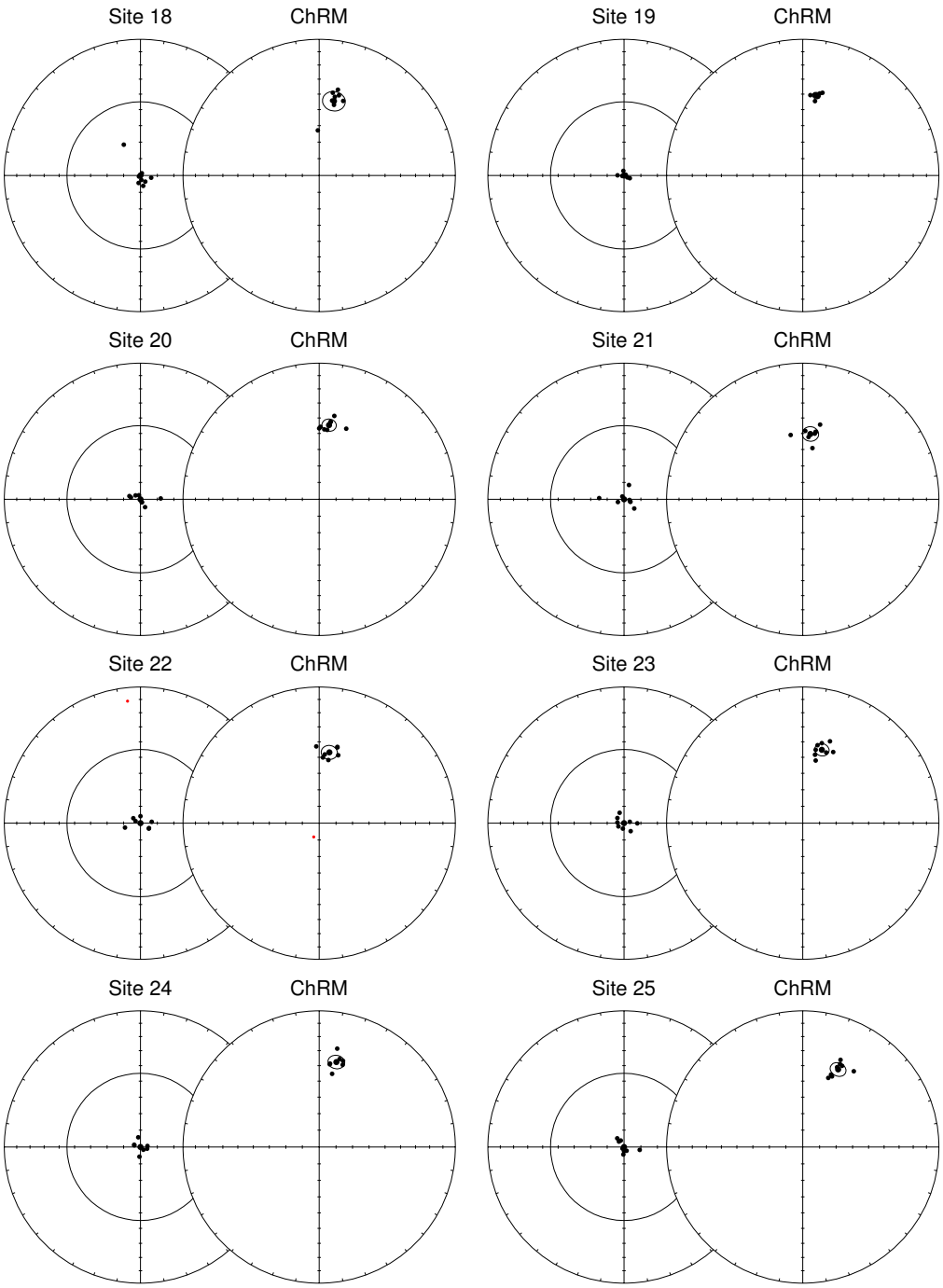
Site 18
ChRM
Site 19
ChRM
Site 20
ChRM
Site 21
ChRM
Site 22
ChRM
Site 23
ChRM
Site 24
ChRM
Site 25
ChRM

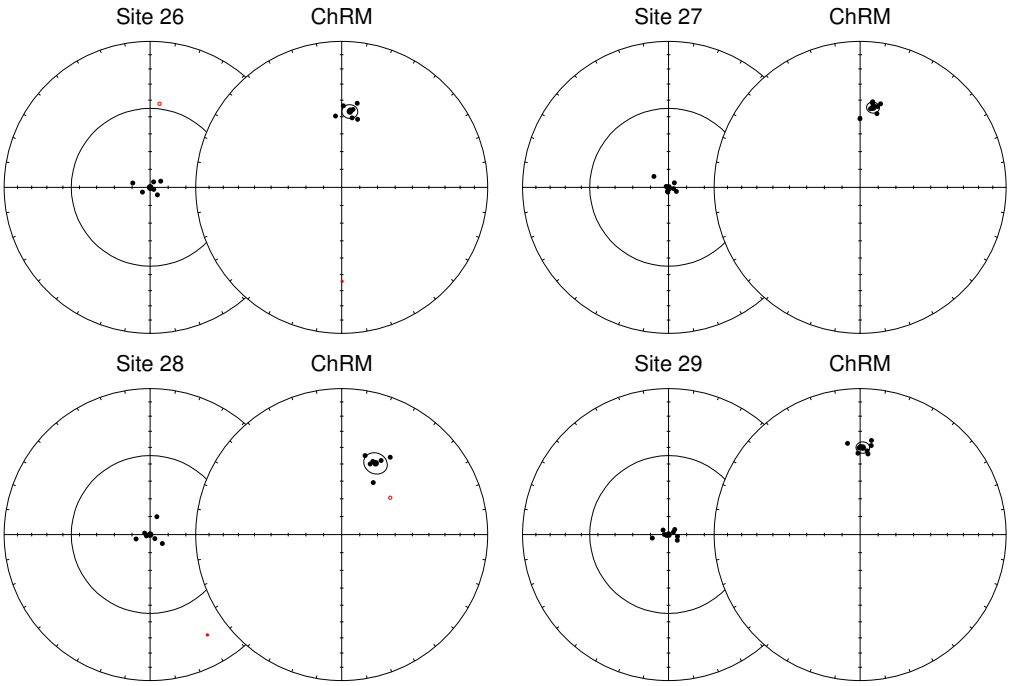
Site 26
ChRM
Site 27
ChRM
Site 28
ChRM
Site 29
ChRM

References

Aitken, M., Allsop, A., Bussell, G., & Winter, M., 1988, Determination of the intensity of the Earth's magnetic field during archaeological times: reliability of the Thellier technique., *Reviews of Geophysics*, 26(1), pp. 3–12.

Ben-Yosef, E., Shaar, R., Tauxe, L., & Ron, H., 2012, A new chronological framework for Iron Age copper production at Timna (Israel), *Bulletin of the American Schools of Oriental Research*, 367, pp. 31–71.

Biggin, A., Strik, G., & Langereis, C., 2009, The intensity of the geomagnetic field in the late-Archaean: New measurements and an analysis of the updated IAGA palaeointensity database, *Earth, Planets and Space*, 61(1), pp. 9–22.

Brown, M., Gratton, M., Shaw, J., Holme, R., & Soler, V., 2009, Microwave palaeointensity results from the Matuyama-Brunhes geomagnetic field reversal, *Physics of the Earth and Planetary Interiors*, 173(1-2), pp. 75–102.

Carracedo, J., Badiola, E., Guillou, H., De La Nuez, J., & Pérez Torrado, F., 2001, Geology and volcanology of la Palma and el Hierro, western Canaries, *Estudios Geologicos*, 57(5-6).

Cassidy, J. & Hill, M., 2009, Absolute palaeointensity study of the Mono Lake excursion recorded by New Zealand basalts, *Physics of the Earth and Planetary Interiors*, 172(3-4), pp. 225–234.

Coe, R. S., Grommé, S., & Mankinen, E. A., 1978, Geomagnetic paleointensities from radiocarbon-dated lava flows on Hawaii and the question of the Pacific nondipole low, *Journal of Geophysical Research: Solid Earth*, 83(B4), pp. 1740–1756.

Cox, A., 1969, Confidence Limits for the Precision Parameter k, *Geophysical Journal of the Royal Astronomical Society*, 17(5), pp. 545–549.

Day, R., Fuller, M., & Schmidt, V., 1977, Hysteresis properties of titanomagnetites: Grain-size and compositional dependence, *Physics of the Earth and Planetary Interiors*, 13(4), pp. 260–267.

De Groot, L., Biggin, A., Dekkers, M., Langereis, C., & Herrero-Bervera, E., 2013a, Rapid regional perturbations to the recent global geomagnetic decay revealed by a new hawaiian record, *Nature Communications*, 4.

De Groot, L., Dekkers, M., & Mullender, T., 2012, Exploring the potential of acquisition curves of the anhysteretic remanent magnetization as a tool to detect subtle magnetic alteration induced by heating, *Physics of the Earth and Planetary Interiors*, 194-195, pp. 71–84.

De Groot, L., Dekkers, M., Visscher, M., & Ter Maat, G., 2014a, Magnetic properties and paleointensities as function of depth in a Hawaiian lava flow, *Geochemistry, Geophysics, Geosystems*, 15(4), pp. 1096–1112.

De Groot, L., Fabian, K., Bakelaar, I., & Dekkers, M., 2014b, Magnetic force microscopy reveals meta-stable magnetic domain states that prevent reliable absolute palaeointensity experiments, *Nature Communications*, 5.

De Groot, L., Mullender, T., & Dekkers, M., 2013b, An evaluation of the influence of the experimental cooling rate along with other thermomagnetic effects to explain anomalously low palaeointensities obtained for historic lavas of Mt Etna (Italy), *Geophysical Journal International*, 193(3), pp. 1198–1215.

Deenen, M., Langereis, C., van Hinsbergen, D., & Biggin, A., 2011, Geomagnetic secular variation and the statistics of palaeomagnetic directions, *Geophysical Journal International*, 186(2), pp. 509–520.

Deenen, M., Langereis, C., Van Hinsbergen, D., & Biggin, A., 2014, Erratum to Geomagnetic secular variation and the statistics of palaeomagnetic directions [Geophysical Journal International, 186, (2011) 509-520], *Geophysical Journal International*, 197(1), p. 643.

Dekkers, M. & Böhnel, H., 2006, Reliable absolute palaeointensities independent of magnetic domain state, *Earth and Planetary Science Letters*, 248(1-2), pp. 507–516.

Di Chiara, A., Tauxe, L., & Speranza, F., 2014, Paleointensity determination from São Miguel (Azores Archipelago) over the last 3ka, *Physics of the Earth and Planetary Interiors*, 234, pp. 1–13.

Dunlop, D. & Xu, S., 1994, Theory of partial thermoremanent magnetization in multidomain grains. 1. Repeated identical barriers to wall motion (single microcoercivity), *Journal of Geophysical Research*, 99(B5), pp. 9005–9023.

Dunlop, D. J., 2002, Theory and application of the Day plot (Mrs/Ms versus Hcr/Hc) 1. Theoretical curves and tests using titanomagnetite data, *Journal of Geophysical Research: Solid Earth*, 107(B3), pp. 2156–2202.

Fabian, K. & Leonhardt, R., 2010, Multiple-specimen absolute paleointensity determination: An optimal protocol including pTRM normalization, domain-state correction, and alteration test, *Earth and Planetary Science Letters*, 297(1-2), pp. 84–94.

Finlay, C. C., Maus, S., Beggan, C. D., Bondar, T. N., Chambodut, A., Chernova, T. A., Chulliat, A., Golovkov, V. P., Hamilton, B., Hamoudi, M., Holme, R., Hulot, G., Kuang, W., Langlais, B., Lesur, V., Lowes, F. J., Lühr, H., Macmillan, S., Mandea, M., McLean, S., Manoj, C., Menvielle, M., Michaelis, I., Olsen, N., Rauberg, J., Rother, M., Sabaka, T. J., Tangborn, A., Toffner-Clausen, L., Thébault, E., Thomson, A. W. P., Wardinski, I., Wei, Z., & Zvereva, T. I., 2010, International Geomagnetic Reference Field: the eleventh generation, *Geophysical Journal International*, 183(3), pp. 1216–1230.

Gallet, Y., Genevey, A., & Le Goff, M., 2002, Three millennia of directional variation of the Earth's magnetic field in western Europe as revealed by archeological artefacts, *Physics of the Earth and Planetary Interiors*, 131(1), pp. 81–89.

Gallet, Y. & Le Goff, M., 2006, High-temperature archeointensity measurements from Mesopotamia, *Earth and Planetary Science Letters*, 241(1-2), pp. 159–173.

Gee, M., Watts, A., Masson, D., & Mitchell, N., 2001, Landslides and the evolution of El Hierro in the Canary Islands, *Marine Geology*, 177(3-4), pp. 271–293.

Guillou, H., Carracedo, J., Pérez Torrado, F., & Rodriguez Badiola, E., 1996, K-Ar ages and magnetic stratigraphy of a hotspot-induced, fast grown oceanic island: El Hierro, Canary Islands, *Journal of Volcanology and Geothermal Research*, 73(1-2), pp. 141–155.

Hill, M. & Shaw, J., 1999, Palaeointensity results for historic lavas from Mt Etna using microwave demagnetization/remagnetization in a modified Thellier-type experiment, *Geophysical Journal International*, 139(2), pp. 583–590.

Holik, J. S., Rabinowitz, P. D., & Austin, J. A., 1991, Effects of Canary hotspot volcanism on structure of oceanic crust off Morocco, *Journal of Geophysical Research: Solid Earth*, 96(B7).

Johnson, C. L., Constable, C. G., Tauxe, L., Barendregt, R., Brown, L. L., Coe, R. S., Layer, P., Mejia, V., Opdyke, N. D., Singer, B. S., Staudigel, H., & Stone, D. B., 2008, Recent investigations of the 05 Ma geomagnetic field recorded by lava flows, *Geochemistry, Geophysics, Geosystems*, 9(4), pp. 1525–2027.

Kissel, C., Guillou, H., Laj, C., Carracedo, J., Nomade, S., Perez-Torrado, F., & Wandres, C., 2011, The Mono Lake excursion recorded in phonolitic lavas from Tenerife (Canary Islands): Paleomagnetic analyses and coupled K/Ar and Ar/Ar dating, *Physics of the Earth and Planetary Interiors*, 187(3-4), pp. 232–244.

Kissel, C. & Laj, C., 2004, Improvements in procedure and paleointensity selection criteria (PICRIT-03) for Thellier and Thellier determinations: Application to Hawaiian basaltic long cores, *Physics of the Earth and Planetary Interiors*, 147(2-3 SPEC.ISS.), pp. 155–169.

Klein, E. M., Smith, D. K., Williams, C. M., & Schouten, H., 2005, Counter-rotating microplates at the Galapagos triple junction., *Nature*, 433(7028), pp. 855 – 858.

Korte, M. & Constable, C., 2005, Continuous geomagnetic field models for the past 7 millennia: 2. CALS7K, *Geochemistry, Geophysics, Geosystems*, 6(2).

Korte, M., Genevey, A., Constable, C., Frank, U., & Schnepp, E., 2005, Continuous geomagnetic field models for the past 7 millennia: 1. A new global data compilation, *Geochemistry, Geophysics, Geosystems*, 6(2).

Laj, C. & Kissel, C., 1999, Geomagnetic field intensity at Hawaii for the last 420 kyr from the Hawaii Scientific Drilling Project core, Big Island, Hawaii, *Journal of Geophysical Research: Solid Earth*, 104(B7), pp. 15 317–15 338.

Laj, C., Kissel, C., Davies, C., & Gubbins, D., 2011, Geomagnetic field intensity and inclination records from Hawaii and the Réunion Island: Geomagnetic implications, *Physics of the Earth and Planetary Interiors*, 187(3-4), pp. 170–187.

Langereis, C., Dekkers, M., De Lange, G., Paterne, M., & Van Santvoort, P., 1997, Magnetostratigraphy and astronomical calibration of the: Last 1.1 Myr from an eastern Mediterranean piston core and dating of short events in the Brunhes, *Geophysical Journal International*, 129(1), pp. 75–94, cited By (since 1996)185.

Leonhardt, R., Heunemann, C., & Krasa, D., 2004, Analyzing absolute paleointensity determinations: Acceptance criteria and the software ThellierTool4.0, *Geochemistry, Geophysics, Geosystems*, 5(12).

Leonhardt, R. & Soffel, H., 2002, A reversal of the Earth's magnetic field recorded in mid-Miocene lava flows of Gran Canaria: Paleointensities, *Journal of Geophysical Research: Solid Earth*, 107(11), pp. EPM 5–1 – 5–11.

Longpré, M.-A., Chadwick, J., Wijbrans, J., & Iping, R., 2011, Age of the El Golfo debris avalanche, El Hierro (Canary Islands): New constraints from laser and furnace 40Ar/ 39Ar dating, *Journal of Volcanology and Geothermal Research*, 203(1-2), pp. 76–80.

Lund, S., Stoner, J., Channell, J., & Acton, G., 2006, A summary of Brunhes paleomagnetic field variability recorded in Ocean Drilling Program cores, *Physics of the Earth and Planetary Interiors*, 156(3-4), pp. 194–204.

Masson, D., 1996, Catastrophic collapse of the volcanic island of Hierro 15 ka ago and the history of landslides in the Canary Islands, *Geology*, 24(3), pp. 231–234.

McFadden, P. & McElhinny, M., 1990, Classification of the reversal test in palaeomagnetism, *Geophysical Journal International*, 103(3), pp. 725–729.

Muxworthy, A., Ji, X., Ridley, V., Pan, Y., Chang, L., Wang, L., & Roberts, A., 2011, Multi-protocol palaeointensity determination from middle Brunhes Chron volcanics, Datong Volcanic Province, China, *Physics of the Earth and Planetary Interiors*, 187(3-4), pp. 188–198.

Muxworthy, A. & Taylor, S., 2011, Evaluation of the domain-state corrected multiple-specimen absolute palaeointensity protocol: A test of historical lavas from Iceland, *Geophysical Journal International*, 187(1), pp. 118–127.

Muxworthy, A. R. & Heslop, D., 2011, A Preisach method for estimating absolute paleofield intensity under the constraint of using only isothermal measurements: 1. Theoretical framework, *Journal of Geophysical Research: Solid Earth*, 116(B4), pp. 2156–2202.

Nagata, T., Arai, Y., & Momose, K., 1963, Secular variation of the geomagnetic force during the last 5000 years, *Journal of Geophysical Research*, 68, pp. 5277–5281.

Pavón-Carrasco, F., Osete, M., & Torta, J., 2010, Regional modeling of the geomagnetic field in europe from 6000 to 1000 B.C., *Geochemistry, Geophysics, Geosystems*, 11(11).

Quidelleur, X. & Valet, J.-P., 1996, Geomagnetic changes across the last reversal recorded in lava flows from La Palma, Canary Islands, *Journal of Geophysical Research B: Solid Earth*, 101(6), pp. 13 755–13 773.

Ravilly, M., Horen, H., Perrin, M., Dyment, J., Gente, P., & Guillou, H., 2001, NRM intensity of altered oceanic basalts across the MAR (21N, 01.5 Ma): a record of geomagnetic palaeointensity variations?, *Geophysical Journal International*, 145(2), pp. 401–422.

Riisager, P. & Riisager, J., 2001, Detecting multidomain magnetic grains in Thellier palaeointensity experiments, *Physics of the Earth and Planetary Interiors*, 125(1-4), pp. 111–117.

Schouten, H., Klitgord, K. D., & Gallo, D. G., 1993, Edge-driven microplate kinematics, *Journal of Geophysical Research: Solid Earth*, 98(B4), pp. 6689–6701.

Selkin, P. & Tauxe, L., 2000, Long-term variations in palaeointensity, *Philosophical Transactions of the Royal Society A: Mathematical, Physical and Engineering Sciences*, 358(1768), pp. 1065–1088.

Shaar, R., Ben-Yosef, E., Ron, H., Tauxe, L., Agnon, A., & Kessel, R., 2011, Geomagnetic field intensity: How high can it get? How fast can it change? Constraints from Iron Age copper slag, *Earth and Planetary Science Letters*, 301(1-2), pp. 297–306.

Singer, B., 2014, A quaternary geomagnetic instability time scale, *Quaternary Geochronology*, 21(1), pp. 29–52.

Spassov, S., Valet, J.-P., Kondopoulou, D., Zananiri, I., Casas, L., & Goff, M., 2010, Rock magnetic property and paleointensity determination on historical Santorini lava flows, *Geochemistry, Geophysics, Geosystems*, 11(7).

Széréméta, N., Laj, C., Guillou, H., Kissel, C., Mazaud, A., & Carracedo, J.-C., 1999, Geomagnetic paleosecular variation in the Brunhes period, from the island of El Hierro (Canary Islands), *Earth and Planetary Science Letters*, 165(3-4), pp. 241–253.

Tauxe, L., 2010, Essentials of Paleomagnetism, University of California Press, ISBN 9780520260313.

Tauxe, L. & Kent, D. V., 2004, A Simplified Statistical Model for the Geomagnetic Field and the Detection of Shallow Bias in Paleomagnetic Inclinations: was the Ancient Magnetic Field Dipolar?, *Geophysical Monograph*, 145, pp. 101–116.

Tauxe, L., Pick, T., & Kok, Y., 1995, Relative paleointensity in sediments: a pseudo-Thellier approach, *Geophysical Research Letters*, 22(21), pp. 2885–2888.

Thellier, E. & Thellier, S., 1959, Sur l'intensité du champ magnétique terrestre dan le passé historique et géologique, *Annales de Geophysique*, 15, pp. 285–376.

Valet, J.-P. & Soler, V., 1999, Magnetic anomalies of lava fields in the Canary islands. Possible consequences for paleomagnetic records, *Physics of the Earth and Planetary Interiors*, 115(2), pp. 109–118.

Xu, S. & Dunlop, D., 1994, Theory of partial thermoremanent magnetization in multidomain grains. 2. Effect of microcoercivity distribution and comparison with experiment, *Journal of Geophysical Research*, 99(B5), pp. 9025–9033.

Yang, T., Li, H., Wu, H., Yang, Z., Zhang, S., & Hyodo, M., 2012, Reliability of relative paleointensity recorded in Chinese loess-paleosol sediments, *Acta Geologica Sinica*, 86(5), pp. 1276–1288.

Yu, Y., Dunlop, D., & Özdemir, O., 2003, Are ARM and TRM analogs? Thellier analysis of ARM and pseudo-Thellier analysis of TRM, *Earth and Planetary Science Letters*, 205(3-4), pp. 325–336.

Yu, Y. & Tauxe, L., 2005, Testing the IZZI protocol of geomagnetic field intensity determination, *Geochemistry, Geophysics, Geosystems*, 6(5).

Yu, Y., Tauxe, L., & Genevey, A., 2004, Toward an optimal geomagnetic field intensity determination technique, *Geochemistry, Geophysics, Geosystems*, 5(2).